IEEE Access
Multidisciplinary | Rapid Review | Open Access Journal

Received 28 June 2024, accepted 20 July 2024, date of publication 29 July 2024, date of current version 6 August 2024.

*Digital Object Identifier 10.1109/ACCESS.2024.3434595*

RESEARCH ARTICLE

# Optimization of a Compact Wearable LoRa Patch Antenna for Vital Sign Monitoring in WBAN Medical Applications Using Machine Learning

**MOHAMED I. WALY[1], (Member, IEEE), JAMEL SMIDA[2,3], (Member, IEEE), MOHSEN BAKOURI[1], (Senior Member, IEEE), BAKHEET AWAD ALRESHEEDI[1], TARIQ MOHAMMED ALQAHTANI[1], KHALID A. ALONZI[4], (Member, IEEE), AND AMOR SMIDA[1,3], (Member, IEEE)**

[1]Department of Medical Equipment Technology, College of Applied Medical Sciences, Majmaah University, Al Majma'ah 11952, Saudi Arabia
[2]College of Applied Science, AlMaarefa University, Riyadh 11597, Saudi Arabia
[3]Microwave Electronics Research Laboratory, Faculty of Sciences of Tunis, University of Tunis El Manar, Tunis 1068, Tunisia
[4]Health Services, Ministry of Defense, Riyadh 12426, Saudi Arabia

Corresponding authors: Mohamed I. Waly (m.waly@mu.edu.sa) and Jamel Smida (jsmida@um.edu.sa)

This work was supported in part by the Deanship of Scientific Research at Majmaah University under Project R-2024-1210.

**ABSTRACT** This study introduces an innovative and compact wearable Long-Range (LoRa) patch antenna developed for monitoring vital signs, with a focus on heart rate and body temperature, in medical applications of Wireless Body Area Networks (WBAN). The antenna functions within the 868 MHz and 915 MHz LoRa bands, filling a notable gap in current literature regarding compact, wearable antennas operating below 1 GHz. Fabricated on a Rogers Duroid RO3003 substrate, the antenna incorporates a U-slot on a conventional rectangular patch, a matching stub, and a partial ground plane to enhance impedance matching and performance efficiency. Furthermore, the antenna displays a bidirectional radiation pattern in the *E*-plane and an omnidirectional pattern in the *H*-plane at both frequencies, achieving a peak gain of 2.12 dBi and a radiation efficiency of 99.8% at 868 MHz. The antenna, measuring $80 \times 60\text{mm}^2$ ($0.23\ \lambda_0 \times 0.17\ \lambda_0$), was designed, simulated, and optimized using CST Microwave Studio (MWS) software. The performance under bending conditions was also assessed, revealing a bending an excellent efficiency with minimal impact on bandwidth and gain. Specific Absorption Rate (SAR) analysis indicated that all values were within the safety limits set by FCC and ICNIRP standards. Supervised regression machine learning models, specifically the ensemble regression model, were employed to predict resonance frequencies based on various antenna parameters, resulting in an R-squared score of 87.68%. This approach significantly reduced the computational time required for full-wave simulations, streamlining the design process. Real-world experimental validation involved open-field testing of the fabricated prototype for WBAN LoRa applications. The performance, evaluated on a LoRa transceiver system utilizing the LoRa SX1276, demonstrated the superior capabilities of the proposed antenna in heart rate and temperature monitoring, with an average RSSI improvement of -5 dBm at various points within a range of up to 1 km. This confirmed its improved signal transmission and reception capabilities in vital sign monitoring. The proposed antenna shows strong performance metrics and significant potential for WBAN in long-range applications, as evidenced by thorough experimental validations.

**INDEX TERMS** LoRa, WBAN, RSSI, wearable, IoT, microstrip patch antenna, machine learning, optimization.

The associate editor coordinating the review of this manuscript and approving it for publication was Tutku Karacolak.

## I. INTRODUCTION

The evolution of the Internet of Things (IoT) has created an era of interconnected devices, facilitating efficient

communication and data exchange. The Internet acts as a global platform transcending geographical, cultural, linguistic, and temporal boundaries, enabling real-time data transmission and connectivity among individuals worldwide. It integrates diverse devices into a unified network, promising an intricate web of interconnected ''smart'' entities like sensors, cameras, and consumer electronics [1], [2], [3]. By 2025, nearly every object could serve as an Internet node, with Cisco estimating 500 billion connected devices by 2030. This proliferation will blur physical and digital boundaries, fostering unparalleled levels of automation, data exchange, and connectivity [4], [5].

Low-power wide-area network (LPWAN) technologies, particularly LoRa (Long Range), are emerging as prominent forces within the interconnected world of IoT. These technologies enable long-distance communication, covering 1-5 km in urban areas and up to 10-40 km in rural areas, with minimal power consumption [6]. LoRa utilizes the LoRaWAN protocol, offering advantages like low cost and efficient chirp spread spectrum (CSS) modulation [7], [8], [9], making it an optimal choice for low-power, long-range wireless communication crucial in IoT deployments [10], [11]. It operates in unlicensed frequency bands globally, with frequencies ranging from 433 MHz to 923 MHz, depending on regional regulations as presented in Table 1, and finds applications in diverse fields, including asset tracking in logistics, manufacturing, and agriculture, as well as smart city initiatives, environmental monitoring, building automation, and utility management.

Wireless Body Area Networks (WBANs) play pivotal roles across various sectors, particularly in healthcare, where real-time monitoring of vital signs and patient activities is crucial for enhancing healthcare outcomes and efficiency. Leveraging the characteristics of LoRa, wherein a LoRa sensor can last for over ten years on a battery without the need for recharge, LoRa-powered WBANs not only facilitate such monitoring but also extend healthcare services to remote and underserved areas, thereby promoting inclusivity in healthcare delivery. Moreover, the adoption of LoRa in WBANs aligns with global sustainability goals, notably Sustainable Development Goal (SDG) 7, by promoting affordable and energy-efficient healthcare solutions. This is critical in healthcare settings where continuous monitoring is imperative while responsibly managing energy resources [12], [13], [14], [15], [16], [17], [18], [19].

**TABLE 1.** LoRa frequency bands by region.

| Region | Frequency Range |
|---|---|
| North America | 915 MHz |
| Asia Pacific | 433 MHz, 923 MHz |
| Europe | 868 MHz |

The effectiveness of LoRa communication depends significantly on antenna performance, highlighting the critical role of antennas in wireless systems. Just as in other wireless technologies, antennas are essential for signal transmission and reception in LoRa. Their design greatly impacts the range, coverage, and reliability of communication. A well-designed antenna promotes efficient signal propagation, leading to extended communication distances and enhanced connectivity in diverse environments. When focusing on WBANs, antennas play an even more critical role due to the specific requirements of wearable and compact devices. WBAN antennas must be designed to be mechanically robust in a straightforward fabrication process. They should offer comfort, compactness, lightweight design, and a comfortable fit for wearability. In the context of LoRa-powered WBANs, specialized antennas are essential to ensure effective communication for vital sign monitoring and other healthcare applications. These antennas must meet stringent criteria for efficiency, reliability, and compatibility with wearable devices, making them a key focus in WBAN system design.

In the last decade, substantial progress has been made in designing microstrip patch antennas specifically for LoRa applications. Researchers have explored various antenna types, materials, and setups to enhance LoRa antenna performance in IoT systems. Notably, a few reported antennas have been specifically aimed for LoRa wearable applications.

A wearable patch antenna was designed to operate at both LoRa 868 MHz and BLE-2.4 GHz frequencies [20]. The antenna's construction included a radiator and ground plane comprising Silver-ink printed fabrics made of polystyrene, with the substrate crafted from neoprene, a blend of synthetic rubbers and textiles. It utilized an aperture-coupled feeding technique for excitation, eliminating the need for a conventional metallic SMA connector known for its bulkiness in wearable antennas. However, this technique induced an additional resonance at 2.4 GHz. The antenna had a size of 150 $mm^2$ and achieved gains of 3.28 dBi and 3.25 dBi at 868 MHz and 2.44 GHz, respectively. While this antenna design showcases innovative techniques and achieves decent gains at the specified frequencies, it may not be optimally suited for WBAN LoRa applications. The size of 150 $mm^2$ may be considered relatively large for wearable applications, where compactness and minimal obtrusiveness are critical. Additionally, the operating frequency of BLE-2.4 GHz is not entirely within the ISM bands below 1 GHz, which are typically preferred for LoRa due to its reduced signal absorption by physical obstacles.

An antenna designed for LoRa applications, specifically a wearable Planar Inverted-F Antenna (PIFA), was introduced in [21]. This antenna featured slots on both the patch and ground plane, enabling dual-band operation at 433 MHz and 868 MHz. With the form factor of $85 \times 169.4 \times 5$ $mm^3$, the antenna exhibited a maximum gain of 1.25 dBi. Critically evaluating this antenna for WBAN LoRa applications where miniaturization and unobtrusive designs are paramount, its size of $85 \times 169.4 \times 5$ $mm^3$ could be a limiting factor. This size could potentially hinder the seamless integration of the antenna into wearable devices, impacting user comfort and overall usability in WBAN environments.

An antenna designed for LPWAN applications in the UHF frequency band adopts an eighth-mode substrate integrated waveguide (EMSIW) configuration [22]. Operating at 867 MHz through the fundamental mode of an EMSIW cavity, this antenna demonstrates a gain measured at −2.7 dB and total dimension of 103.8 mm × 94.2 mm. When assessing this antenna for WBAN LoRa applications, its size and relatively low gain are notable considerations. While the use of an EMSIW configuration and high isolation from the human body are advantageous, the antenna's dimensions may pose challenges for integration into wearable devices, where compactness and unobtrusiveness are crucial. Additionally, the measured gain of -2.7 dB may indicate suboptimal performance in terms of signal strength and coverage, potentially limiting its effectiveness in WBAN environments requiring reliable and robust communication.

A dual-band wearable antenna, detailed in [23], is introduced as a textile-based design utilizing an SIW cavity. The miniaturization of the antenna is achieved by capitalizing on the inherent symmetry of the magnetic field within a square SIW cavity, leading to an eighth-mode SIW configuration and reducing the size to $\frac{1}{8}$ of the full square cavity. This design is specifically targeted for LoRa applications, covering both European (863-870 MHz) and North American (902-928 MHz) UHF LoRa bands. However, the antenna's dimensions are 125 mm × 120 mm. In testing, the antenna displayed a measured gain of −1.3 dBi at 867 MHz and −0.6 dBi at 915 MHz when placed near a liquid body phantom. Critiquing this antenna design for WBAN LoRa applications, its size remains a concern despite efforts to miniaturize it through the SIW cavity configuration. The dimensions of 125 mm × 120 mm may still be considered relatively large for wearable devices, potentially impacting comfort and usability. Additionally, the measured gains of −1.3 dBi and −0.6 dBi suggest a lower-than-desired performance in terms of signal strength, which could limit the antenna's effectiveness in WBAN environments requiring robust and reliable communication.

A dual-band footwear textile antenna aimed for LoRa off-body communication is discussed in [24]. This antenna, engineered for flexibility and conformity to the heel, operates across the 433 MHz, 868 MHz, and 915 MHz bands. By employing slotted and loaded elements, it achieves dual-band performance with ample bandwidths of 51 MHz and 257 MHz in the lower and upper bands, respectively. Both simulation and measurement results showcase an omnidirectional radiation characteristics suitable for off-body communication. Critically evaluating this antenna, its size of 95 mm × 65 mm is comparatively larger.

A novel and compact wearable patch antenna, designed to cover the 915 MHz and 868 MHz frequencies for LoRa applications in Asia, North America and Europe is presented in this paper. The antenna boasts a compact design measuring 80 × 60 × 0.5 $mm^3$. This size is approximately equivalent to a standard credit card, addressing common limitations seen in other designs such as low gain, large profiles, single-frequency operation, and low efficiency. A unique aspect of this work is the integration of machine learning techniques for resonance frequency prediction during antenna optimization. This novel approach sets it apart from previous works, often relying on full-wave simulation software as the primary optimization tool without exploring machine learning-based optimization. Another unique aspect of this work is the In-depth characterization conducted in a practical setting, particularly with LoRa systems, to evaluate the performance of our designed antenna in vital sign monitoring. This aspect is often overlooked in prior designs, highlighting the thoroughness and applicability of the study.

To assess the proposed antenna's performance thoroughly, the study includes an experimental setup comprising a LoRa device and sensors, specifically for WBAN LoRa systems used in vital sign monitoring. This setup enables meticulous evaluation, with a specific focus on Received Signal Strength Indicators (RSSI) to gauge the antenna's effectiveness in this critical application domain.

The key contributions of this paper can be summarized as follows:

1) To the best of our knowledge, this study presents the most compact wearable patch antenna for LoRa applications, addressing a significant gap in current research.
2) The antenna optimization was performed using machine learning techniques, which are significantly faster than traditional methods relying on full-wave simulation software such as CST MWS. This innovative approach has been underexplored in the context of wearable antennas.
3) An equivalent circuit model for the antenna was developed and validated against simulation and prototype measurement results. This validation method is rarely used in existing literature, adding robustness to our findings.
4) The paper provides a detailed analysis of the antenna's performance under bending conditions on human phantom and SAR evaluation when placed near or on the human body. Simulated results were rigorously compared with measured data, addressing aspects often neglected in previous studies.
5) Extensive real-world testing of the prototype antenna on LoRa system for heart rate and temperature monitoring was conducted. This approach is seldom explored in prior research on wearable LoRa patch antennas.

This paper is presented in the following manner: Section II details the design evolution of the antenna, outlining the iterative development process. Section III conducts parametric studies using CST MWS to optimize the antenna's performance. Section IV explores machine learning (ML)-based optimization, utilizing supervised regression machine learning models to predict resonance frequencies and enhance design efficiency. Section V introduces an equivalent circuit model of the proposed antenna to provide a simplified

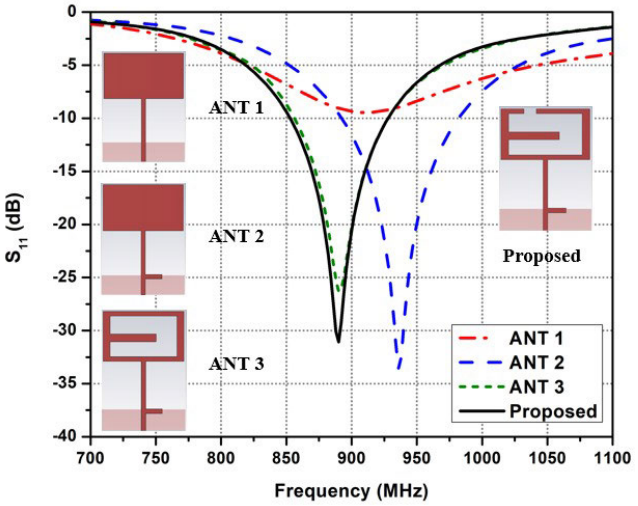


**FIGURE 1.** Illustration of the evolution steps for the proposed antenna.

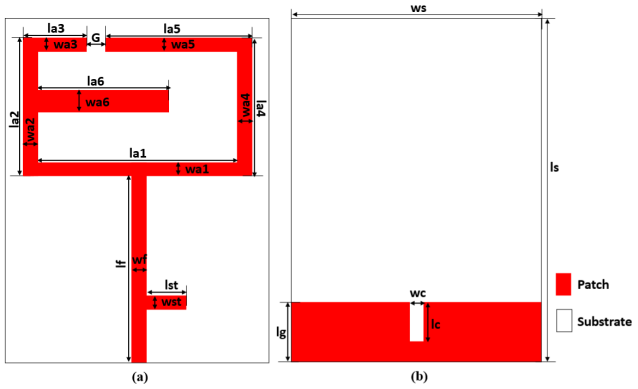


**FIGURE 2.** Geometry of the proposed LoRa wearable antenna depicting its (a) Front and (b) Back views.

representation of its electrical behavior. Section VI presents the results and analysis of performance metrics such as $S_{11}$, current distribution, efficiency, radiation pattern, and gain, for both simulations and measurements. Section VII explores how the antenna's performance is affected by bending. Section VIII conducts SAR analysis to ensure safety standards are met when the antenna is worn on the human body. Section IX assesses the antenna's performance near the human body, considering real-world application scenarios. Section X includes experimental validation with real-world testing of the fabricated prototype, featuring open-field performance evaluations. Section XI evaluates the performance of the proposed system when integrated with a LoRa device, focusing on long-range communication capabilities. Section XII summarizes the findings and highlights the potential applications of the proposed antenna in WBAN medical applications.

## II. ANTENNA'S DESIGN EVOLUTION

The development of the proposed LoRa wearable antenna involved an iterative process aimed at optimizing its performance for LoRa applications. The antenna as shown in Fig. 1 underwent several design iterations, each contributing to its overall functionality and effectiveness.

The initial design of the proposed antenna, labeled as ANT 1, featured a conventional rectangular patch antenna fed by a 50 Ω microstrip transmission line. The patch's dimensions, including its length and width, were computed using the transmission line model approach as outlined in [25]. The substrate material chosen was Rogers Duroid RO3003$^{TM}$, characterized by a loss tangent coefficient of 0.0013, a dielectric constant of 3, and a height of 0.5 mm. This initial design using CST MWS software laid the foundation for subsequent improvements.

Recognizing the importance of impedance matching for efficient power transfer, Antenna 2 (ANT 2) introduced a matching stub to improve the impedance match between the antenna and the feed line. The dimensions of this matching stub, denoted as $l_m \times w_m$, were carefully optimized to enhance return loss and minimize signal reflection. Antenna 3 (ANT 3) was developed to cover both the 868 MHz and 915 MHz LoRa communication frequencies. This design incorporated a U-slot cut into the rectangular patch, which effectively lowered the resonant frequency, enabling operation within the desired frequency bands. Building upon the insights gained from the previous iterations, the final proposed antenna design further refined the patch geometry for improved performance. An additional slot was strategically added at the top left corner of the rectangular patch, enhancing control over current distribution and achieving a return loss value $< -10$ dB which covered both 868 MHz and 915 MHz for LoRa communications. The optimized design and dimensions of the proposed LoRa wearable antenna are visually represented in Fig. 2, with detailed parameter values provided in Table 2.

The innovative aspect of the proposed LoRa wearable antenna lies in the use of meandered monopoles to achieve lower resonance frequencies while maintaining small antenna dimensions. Ordinarily, the size of a conventional antenna at 868 MHz would have been significantly larger, but the meandered structure allows for compactness without compromising performance. This unique design approach enables the antenna to operate efficiently at the desired LoRa frequencies of 868 MHz and 915 MHz, making it suitable for wearable applications where space is limited. The meandered monopole design not only reduces the overall size of the antenna but also enhances its functionality, demonstrating a significant advancement in antenna miniaturization and performance optimization.

## III. PARAMETRIC STUDIES USING CST MWS

In this section, critical parameters of the proposed antenna such as matching stub width ($W_m$), matching stub length ($l_m$), ground plane length ($l_g$), $U$-slot dimensions ($l_{a5}$, $l_{a6}$, $w_{a1}$, $w_{a4}$), feedline width ($w_f$), and the width ($G$) of the second slot were systematically examined to understand their impact on the antenna's performance. This analysis aims to identify optimal values for these parameters using CST MWS,

**TABLE 2. Dimensions of parameters in the proposed antenna.**

| Parameter | Dimension (mm) | Parameter | Dimension (mm) |
|---|---|---|---|
| lf | 46 | wf | 3 |
| la1 | 58 | wa1 | 3 |
| la2 | 33 | wa2 | 2 |
| la3 | 15 | wa3 | 5 |
| la4 | 33 | wa4 | 5 |
| la5 | 35 | wa5 | 3 |
| la6 | 33 | wa6 | 5 |
| Lm | 12 | wm | 3 |
| lc | 10 | wc | 3 |
| ls | 80 | ws | 60 |
| lg | 14 | G | 8 |

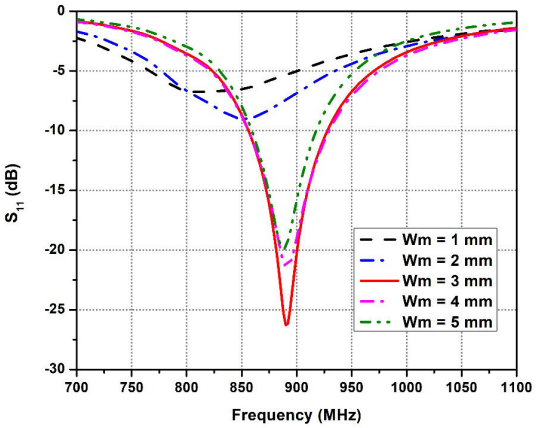


**FIGURE 3. Optimization of $w_m$ and its effect on $S_{11}$.**

enabling the fine-tuning of the antenna design for enhanced efficiency, broader frequency coverage, and improved signal reception in LoRa applications. Additionally, another aim is to compare the results of these optimizations with those carried out using machine learning in Section IV.

The initial antenna design (ANT 1) exhibited suboptimal impedance matching, prompting the introduction of a matching stub in ANT 2. Parametric studies on $W_m$ and $l_m$ as depicted in Fig. 3 and Fig. 4 respectively revealed optimal values of $W_m = 3$ mm and $l_m = 12$ mm, achieving resonance at both 868 MHz and 915 MHz frequencies essential for LoRa communication.

Similarly, parametric studies as shown in Fig. 5 and Fig. 6 optimized the $U$-slot dimensions ($l_{a1} = 58$ mm, $l_{a6} = 33$ mm) respectively to manipulate current distribution on the antenna, enhancing resonant characteristics for LoRa applications. Additionally, varying $L_g$ from 12 mm to 16 mm as shown in Fig. 7 identified $L_g = 14$ mm as optimal, ensuring stable grounding and resonant frequency achievement.

## IV. OPTIMIZATION OF THE ANTENNA USING MACHINE LEARNING

Advancements in machine Learning (ML) within the context of electromagnetics (EM) are revolutionizing antenna design methodologies. Traditional approaches, such as parameter sweeps using full-wave simulation software like CST MWS, have proven laborious due to the intricate nature of modern antennas and their performance demands. This complexity

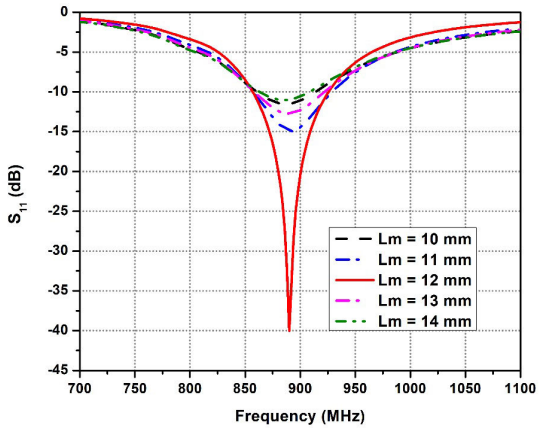


**FIGURE 4. Optimization of $l_m$ and its effect on $S_{11}$.**

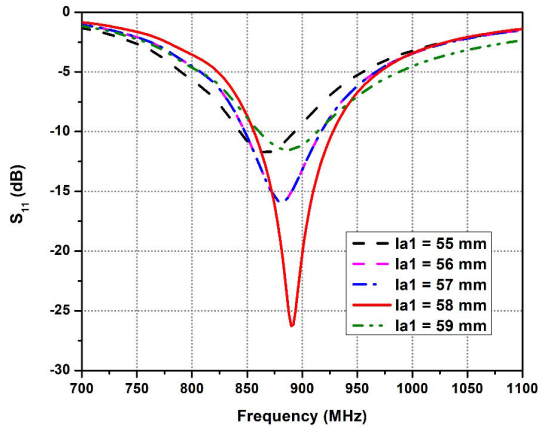


**FIGURE 5. Optimization of $l_{a1}$ and its effect on $S_{11}$.**

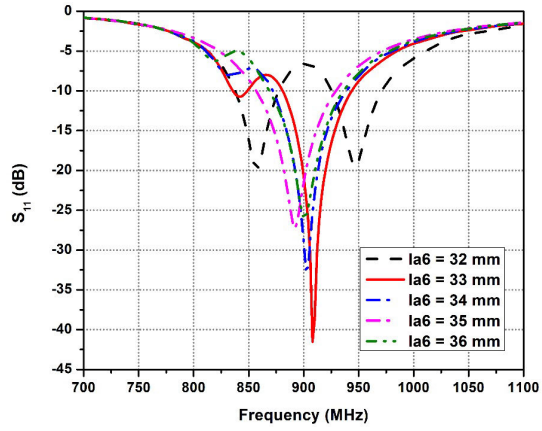


**FIGURE 6. Optimization of $l_{a6}$ and its effect on $S_{11}$.**

often necessitates the use of numerical analysis techniques like the Finite Difference Time Domain (FDTD), Methods of Moments (MoM), and Finite Element Method (FEM), with 3D EM simulators such as ADS, HFSS, and CST programs. However, these software tools can be time-consuming, particularly for sophisticated antenna designs. Recognizing this challenge, researchers are exploring the integration of deep learning (DL) and ML algorithms to streamline antenna design processes. ML and DL, both branches of artificial

**TABLE 3.** Comparison of various regression models.

| Model | Key Features | Applications | Ref. |
|---|---|---|---|
| Linear Regression (LR) | Simple and easy to understand; Assumes linear correlation between variables | Trend analysis, prediction in well-organized data | [27] |
| Efficient Linear Regression (ELR) | Maximizes predictive performance without sacrificing processing efficiency; Utilizes algorithmic improvements and computational shortcuts | Regression tasks, high-dimensional scenarios | [28] |
| Decision Trees Regression (DTR) | Flexible and handles non-linear correlations; Divides feature space based on input variable values to reduce impurity or increase information gain | Regression, classification tasks | [29] |
| Support Vector Machines Regression (SVMR) | Optimizes margin between classes or fits data with minimal error; Operates well with high-dimensional data and is noise-resistant | Classification, regression applications | [30] |
| Gaussian Process Regression (GPR) | Bayesian approach providing uncertainty estimates; Responds to intricate data patterns | Regression tasks, uncertainty estimation | [30] |
| Kernel Approximation Regression (KAR) | Operates in high-dimensional feature spaces; Adapts to various data patterns through different kernel functions | High-dimensional data, various data patterns | [31] |
| Ensemble Tree Regression (ETR) | Combines multiple models for improved performance and generalization; Less prone to overfitting and instability compared to individual models | Improved predictive performance, generalization | [32] |

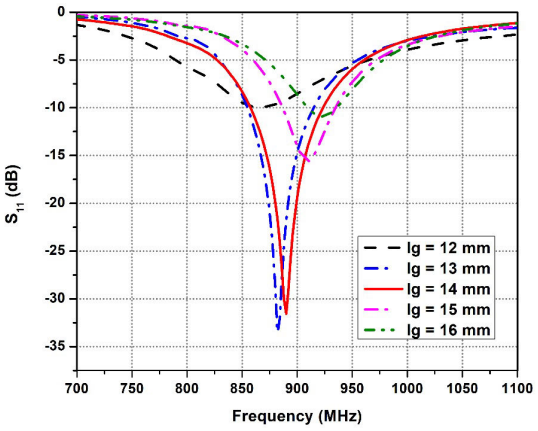


**FIGURE 7.** Optimization of $l_g$ and its effect on $S_{11}$.

intelligence, offer the potential to significantly accelerate design iterations while maintaining high accuracy, presenting a promising avenue for enhancing design workflows and predicting antenna behavior [26]. In this section, we examine how ML techniques are employed to predict the resonant frequencies of the proposed antenna. These predictions are then compared with the simulated results obtained using CST MWS.

### A. SELECTION OF THE DATA SETS AND THE ALGORITHM

For any prediction to be made, there must be sets of input data to feed the system. The proposed antenna was modeled in CST MWS and optimized using the Trust Region framework and Genetic algorithm. Datasets of critical parameters of the proposed antenna model from this optimization were extracted. The input variables included $W_m$, $l_m$, $l_g$, $l_{a1}$, $l_{a6}$, and each corresponding output variable (resonant frequency) was obtained for each optimization run. A total of 8007 sets of inputs and outputs were used for resonance frequency prediction. The available data was divided into 90% for training and 10% for validation. A separate 10% dataset was obtained and used for testing to substantiate the robustness of the model. In this work, the data preparation and extraction process, illustrated in Fig. 8, involves three key stages. First, the proposed wearable antenna for LoRa applications is designed and optimized in CST to achieve the desired frequency. Next, a parameter study is conducted to generate extensive datasets suitable for regression analysis using machine learning algorithms. Finally, the simulation results, including return loss ($S_{11}$), are exported from CST for further analysis.

The ML algorithms utilized for optimization and prediction included Linear Regression (LR), Efficient Linear Regression (ELR), Decision Trees Regression (DTR), Support Vector Machines Regression (SVMR), Gaussian Process Regression (GPR), Kernel Approximation Regression (KAR), and Ensemble Tree Regression (ETR). Each algorithm offers unique advantages and capabilities in handling regression tasks, as summarized in Table 3.

The flowchart in Fig. 9 illustrates a systematic process for predicting resonance frequency using various regression algorithms. These algorithms are trained using the training dataset, allowing them to learn the relationship between the the target variable (resonance frequency) and the input

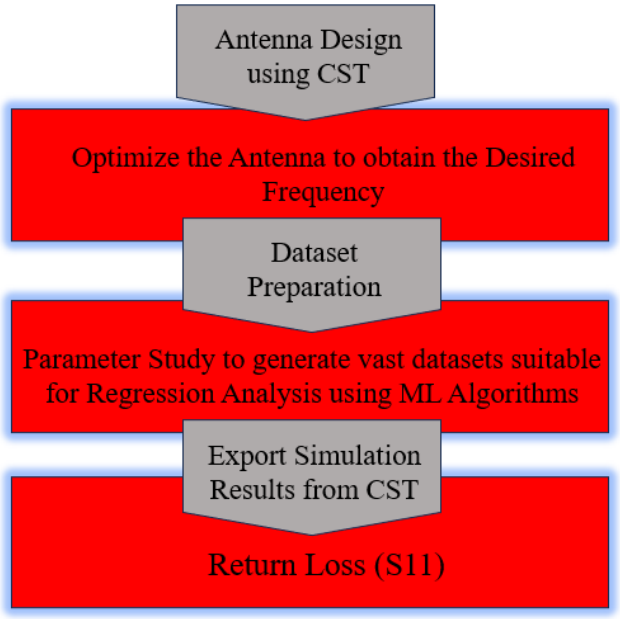


**FIGURE 8.** Workflow for data collection for ML analysis.

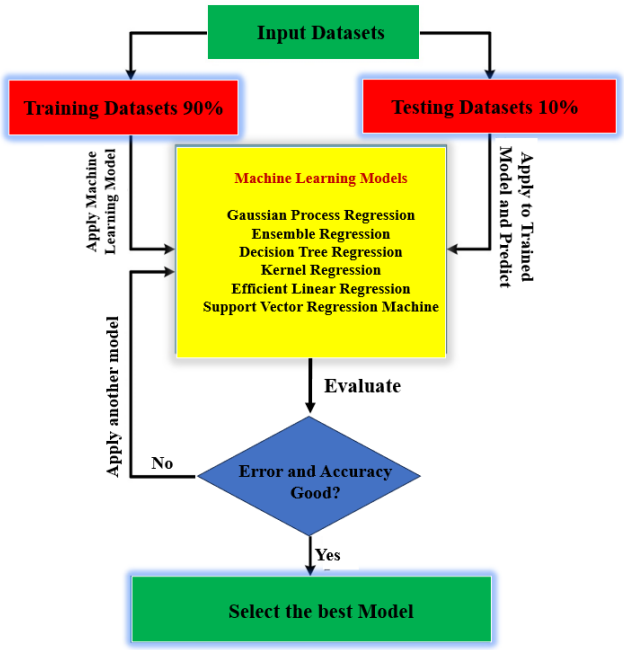


**FIGURE 9.** Flowchart illustrating the process of the prediction.

features. After the training, the models are evaluated based on their performance on the testing dataset. This evaluation involves applying the trained models to the testing data to predict resonance frequencies and comparing these predictions with the actual values. Key performance metrics, such as error and accuracy, are calculated to assess how well each model has performed. The decision point in the flowchart checks whether the models' error and accuracy metrics meet predefined criteria. If a model's performance is satisfactory, indicated by low error and high accuracy, it is selected as the best model for predicting resonance frequencies. If the performance is not satisfactory, another model is applied, and this iterative process continues until the model with the best performance metrics is identified. Finally, the best-performing model is used to make predictions on new data. This involves applying the input datasets to the model to predict resonance frequency based on the learned patterns. This structured approach ensures that the most effective machine learning model is selected, leveraging the strengths of various regression algorithms to achieveccurate and reliable predictions. The systematic evaluation and selection process ensures that the chosen model provides the best possible performance on unseen data, leading to robust and precise resonance frequency predictions.

### B. METRICS FOR PERFORMANCE MEASUREMENT IN REGRESSION ANALYSIS

In regression analysis, the key measure of success hinges on minimizing the discrepancies between predicted and actual values, often referred to as errors. To assess the effectiveness of each model in this regard, a comprehensive evaluation using various statistical metrics was conducted. A comprehensive set of seven (7) statistical indicators were employed to assess the performance of the algorithms, and their results were compared. The following statistical measures were utilized for the assessment: Root Mean Squared Logarithmic Error (RMSLE), Mean Squared Logarithmic Error (MSLE), Mean Squared Error (MSE), Root Mean Squared Error (RMSE), Mean Absolute Error (MAE), Mean Absolute Percentage Error (MAPE), and variance score (R-squared). Table 4 presents the features of each of these metrics.

### C. ML BASED PREDICTION ANALYSIS

In assessing the performance of various machine learning algorithms for predictive modeling, a comprehensive evaluation was conducted utilizing the aforementioned seven (7) statistical metrics. Multiple iterations were executed to determine the most effective algorithm for prediction within the given dataset. It is acknowledged that no single algorithm inherently outperforms others; rather, the selection of an algorithm depends on the specific characteristics of the problem being addressed. Upon analyzing the results presented in Table 5, several key observations emerged:

Optimal predictive performance is indicated by lower values of MAE, MSE, and RMSE, reflecting reduced error in predictions. A higher R-squared value is indicative of a better overall fit of the model to the data. Given these criteria, the Ensemble Regression model emerged as the most favorable. Its superior performance is evidenced by its lowest MAE, relatively modest MSE and RMSE, and notably high R-squared value compared to other models evaluated. Ensemble methods, known for their ability to integrate diverse models for improved performance, demonstrated their efficacy in producing a more accurate and robust predictive model for this particular dataset. Thus, based on the

**TABLE 4.** Summary of evaluation metrics for regression analysis.

| Metric | Features | Equation |
|---|---|---|
| **Mean Absolute Error (MAE)** | Measures the average magnitude of the errors without considering their direction | $\frac{1}{n}\sum_{i=1}^{n}\lvert y_i - \hat{y}_i\rvert$ |
| **Mean Squared Error (MSE)** | Measures the average squared difference between predicted and actual values, penalizing larger errors | $\frac{1}{n}\sum_{i=1}^{n}(y_i - \hat{y}_i)^2$ |
| **Root Mean Squared Error (RMSE)** | Provides an error measure in the same units as the target variable, emphasizing larger errors | $\sqrt{\frac{1}{n}\sum_{i=1}^{n}(P_i - O_i)^2}$ |
| **Coefficient of Determination ($R^2$)** | Indicates the proportion of variance in the dependent variable explained by the independent variables | $1 - \frac{\sum_{i=1}^{N}(y_i - \hat{y}_i)^2}{\sum_{i=1}^{N}(y_i - \bar{y})^2}$ |
| **Mean Squared Logarithmic Error (MSLE)** | Focuses on the relative differences between actual and predicted values using logarithms | $\frac{1}{n}\sum_{i=1}^{n}(\log(1+y_i) - \log(1+\hat{y}_i))^2$ |
| **Root Mean Squared Logarithmic Error (RMSLE)** | Provides an error measure in the same scale as the target variable, useful for varying scales | $\sqrt{\frac{1}{n}\sum_{i=1}^{n}(\log(1+y_i) - \log(1+\hat{y}_i))^2}$ |
| **Mean Absolute Percentage Error (MAPE)** | Expresses errors as a percentage of actual values, useful for interpreting model accuracy in percentage terms | $\frac{1}{n}\sum_{i=1}^{n}\left\lvert\frac{y_i - \hat{y}_i}{y_i}\right\rvert \times 100\%$ |

**TABLE 5.** Comparison of performance of various regression models.

| Model | MAE (%) | MSE (%) | MSLE (%) | RMSLE (%) | RMSE (%) | R-squared (%) |
|---|---|---|---|---|---|---|
| Gaussian Process Regression | 0.6133 | 1.3745 | 0.7741 | 0.4975 | 1.1724 | 88.7644 |
| Ensemble Regression | 0.3991 | 1.5075 | 0.5535 | 0.7471 | 1.2278 | 87.6776 |
| Decision Tree Regression | 0.4198 | 1.5832 | 0.5552 | 0.7482 | 1.2582 | 87.0590 |
| Decision Tree Regression 2 | 0.4205 | 1.5833 | 0.2315 | 0.4823 | 1.2583 | 87.0577 |
| Kernel Regression | 1.2357 | 8.6088 | 0.2615 | 0.5907 | 2.9341 | 29.6303 |
| SVM Regression | 1.4278 | 12.7388 | 1.2274 | 1.4895 | 3.5691 | -4.1292 |
| Efficient Linear Regression | 1.6519 | 13.5092 | 0.3378 | 1.4183 | 3.6755 | -10.4264 |

comprehensive analysis of the provided metrics as depicted in Fig. 10 and Fig. 11, the Ensemble Regression model stands out as the optimal choice for regression modeling in this context. The negative R-squared values observed in the SVM Regression and Efficient Linear Regression models signify that these models exhibit predictive performance inferior to a horizontal line, indicating an inability to capture the variance in the dependent variable. Possible factors contributing to this suboptimal performance might be violations of regression assumptions.

Fig. 12 illustrates some predicted $S_{11}$ plots of the proposed antenna alongside the actual simulated plots for various regression models. The Ensemble Regression model stands out as the best performer, closely matching the actual values, followed by Gaussian Process Regression. In contrast, the worst performance is observed in the SVM Regression and Efficient Linear Regression models, as indicated by their significantly higher error metrics. These models enable the approximate determination of the $S_{11}$ of the proposed wearable antenna by merely inputting the antenna parameters, thereby eliminating the need to use CST Studio Suite or other full-wave simulation software such as HFSS or FEKO for modeling the antenna from scratch. Additionally, this prediction approach significantly reduces the time required for conventional optimization methods.

## V. CIRCUIT MODEL ANALYSIS OF THE PROPOSED ANTENNA

An equivalent circuit can be used to model characteristics such as resonant frequency, bandwidth, and impedance

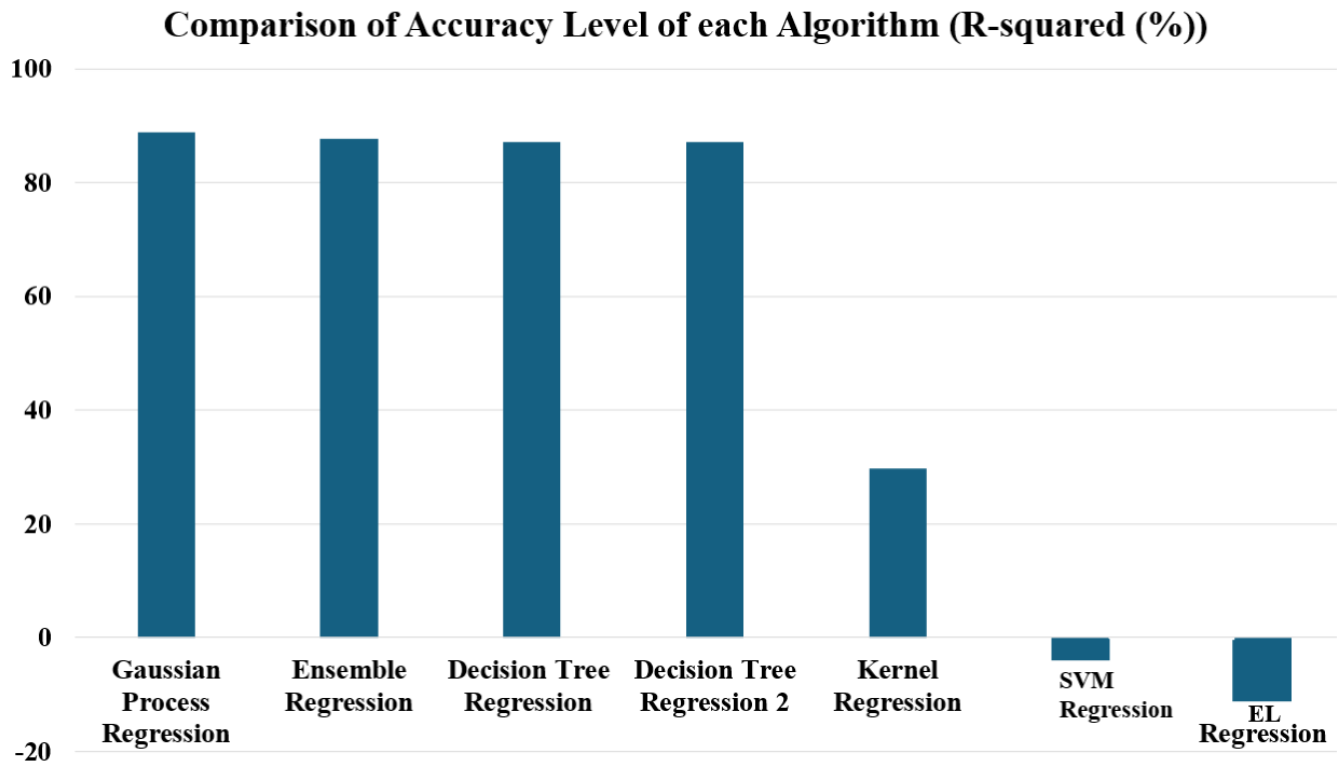


**FIGURE 10.** Illustration of bar charts of errors for different algorithms.

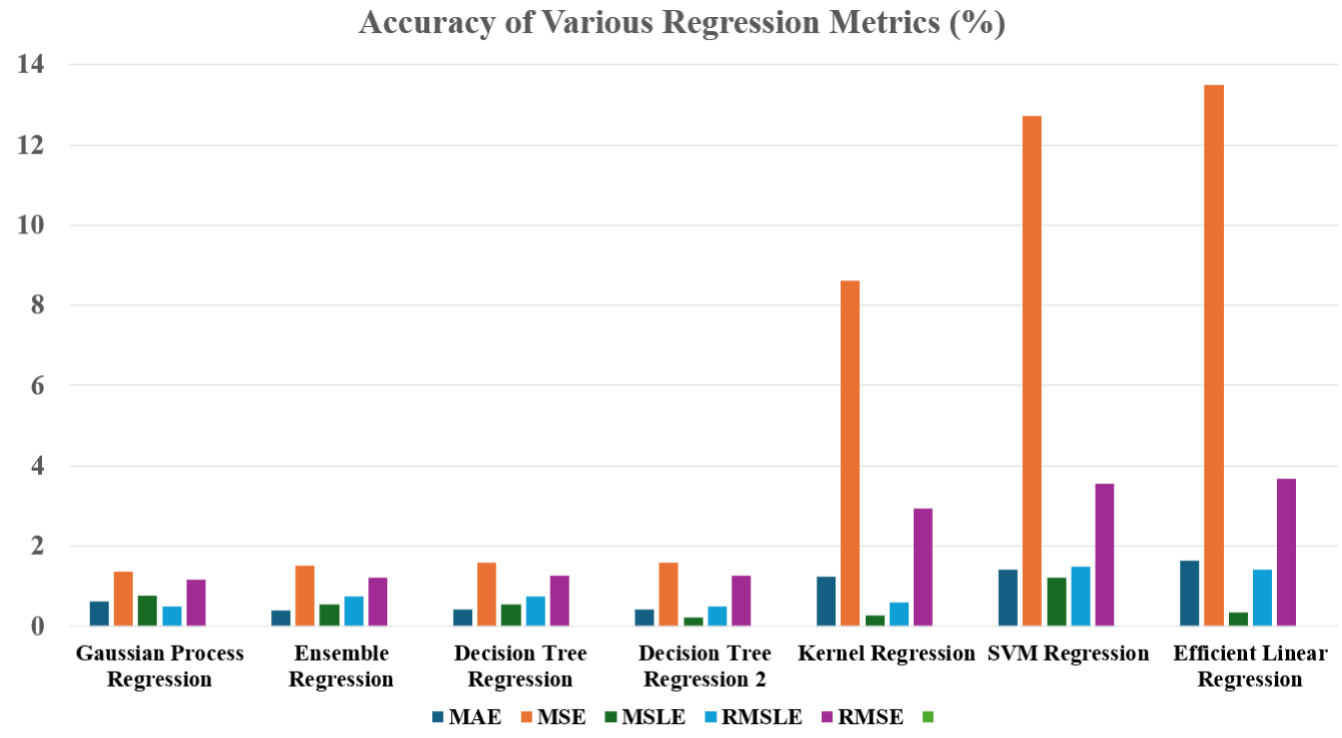


**FIGURE 11.** Illustration of bar charts of accuracy levels of each algorithm.

matching [33] of an antenna. This guides the design process before conducting detailed simulations or measurements. Fig.13 depicts the evolution of the equivalent circuit of the proposed antenna. $S_{11}$ data will be extracted from the equivalent circuit model using ADS software and compared with simulated data from CST MWS® software.

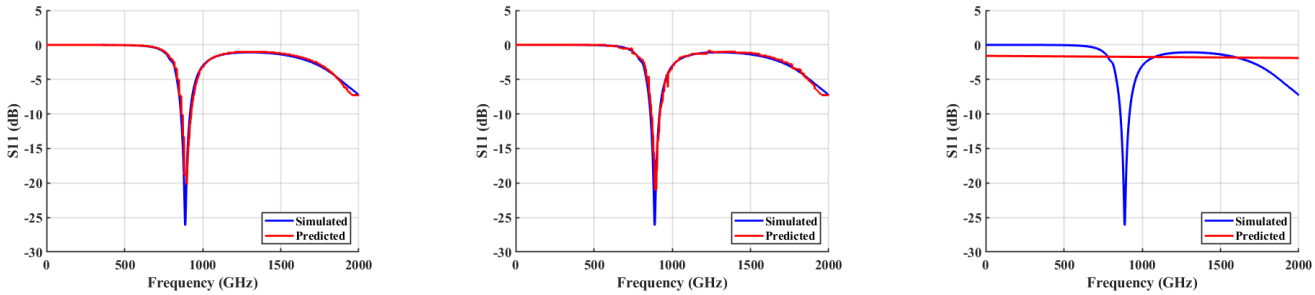


**FIGURE 12.** Comparison of some simulated and predicted $S_{11}$ (a) Ensemble regression (b) Gaussian process regression and (c) Efficient linear regression.

**TABLE 6.** Comparison of antennas optimized using machine learning techniques.

| Ref | Year | ML Model | Antenna Type | Optimization Criteria | Performance Metrics | Results & Observations |
|---|---|---|---|---|---|---|
| [26] | 2023 | Random forest | Base station | Axial Ratio Bandwidth | AR Bandwidth | Enhanced prediction accuracy, Improved AR bandwidth by 41%. |
| [30] | 2024 | Gaussian Process Regression | Monopole Antenna | Resonant frequency prediction | Return loss | Gaussian process regression has the best performance among other regression models. |
| [38] | 2023 | Linear and ridge regression | Quasi-Yagi-Uda | Resonance frequency, directivity | Return loss, directivity | Ridge regression performed well in predicting frequency, whereas the linear regression model exhibited the lowest error and highest accuracy in predicting directivity. |
| [39] | 2024 | Convolutional Neural Network (CNN), Gaussian Process Regression (GPR) | Patch Antenna | Antenna geometry optimization | Reduction in mutual coupling | Improved convergence speed. |
| [40] | 2024 | Gaussian Process Regression | Patch Antenna | Return loss, Efficiency | Resonant point, Efficiency | Gaussian process regression has comparatively the lowest error. |
| **This work** | | Ensemble regression | Monopole Antenna | Resonant frequency prediction | Return loss | Ensemble regression has the best performance, it has significantly reduced the computational time required for antenna optimization. |

Generally, a microstrip patch antenna is analogous to an open-ended transmission line. The equivalent circuit model of ANT 1, designed and simulated using ADS software, can be represented by parallel lumped elements: resistance (R1), inductance (L1), and capacitance (C1). The values for R1, L1, and C1 are calculated using equations from references [34] and [35]. ANT 2, which introduced a matching stub to improve impedance matching between the antenna and the feed line, is represented by the parallel lumped elements R2, L2, and C2, as shown in Fig.13(a). ANT 3 was developed to cover both the 868 MHz and 915 MHz LoRa communication frequencies. This design incorporated a U-slot cut into the rectangular patch, effectively lowering the resonant frequency to operate within the desired bands; they can be represented as additional series inductance ($\Delta L$) and capacitance ($\Delta C$) in the equivalent circuit of the patch antenna and can be calculated using equations from [36] and [37]. An additional slot was strategically added at the top left corner of the rectangular patch, enhancing control over current distribution and achieving a return loss value of less than $-10$ dB, covering both 868 MHz and 915 MHz for LoRa communications, as shown in Fig.13(b). The equivalent circuits of the rectangular patch, matching stub, U-slot, and additional slot are combined via mutual inductance (Lm) and mutual capacitance (Cm), as illustrated in Fig.13(c). The values of each element are listed in Table 7.

## VI. RESULTS AND ANALYSIS

To validate the design and simulations of the proposed antenna, a prototype of the antenna was fabricated, as shown in Fig. 14. The antenna's characterization was carried out using an anechoic chamber and a Keysight Vector Network Analyzer (VNA) with model N5234B as depicted in Fig. 15. The $S_{11}$ parameters were measured with the VNA, as illustrated in Fig. 15(a). Furthermore, far-field measurements, including gain and radiation patterns were conducted in the

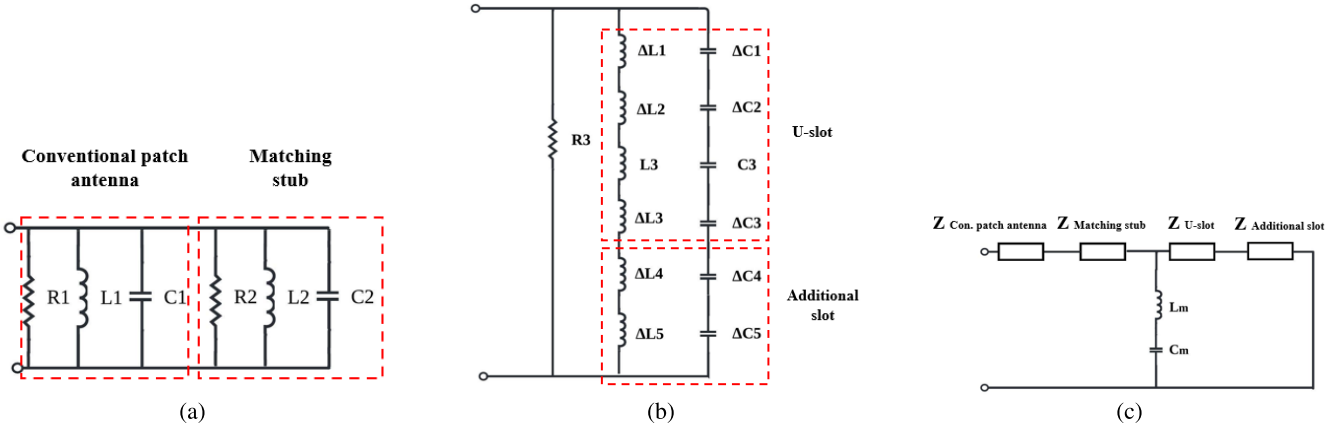


**FIGURE 13.** Equivalent circuit (a) Patch antenna (b) Additional slots (c) Proposed antenna.

**TABLE 7.** Values of lumped elements.

| Lumped Element | R1 (Ω) | L1 (nH) | C1 (pF) | R2 (Ω) | L2 (nH) | C2 (pF) | R3 (Ω) | L3 (nH) | C3 (pF) | $\Delta L1$ (nH) | $\Delta L2$ (nH) |
|---|---|---|---|---|---|---|---|---|---|---|---|
| Values | 51.1 | 1.7 | 2.5 | 49.8 | 7.9 | 11.4 | 51.8 | 9.7 | 3.8 | 113 | 78 |

| Lumped Element | $\Delta L3$ (nH) | $\Delta L4$ (nH) | $\Delta L5$ (nH) | $\Delta C1$ (pF) | $\Delta C2$ (pF) | $\Delta C3$ (pF) | $\Delta C4$ (pF) | $\Delta C5$ (pF) | Lm (nH) | Cm (pF) |
|---|---|---|---|---|---|---|---|---|---|---|
| Values | 135 | 147 | 63 | 1.4 | 241 | 164 | 0.5 | 112 | 1.3 | 3.5 |

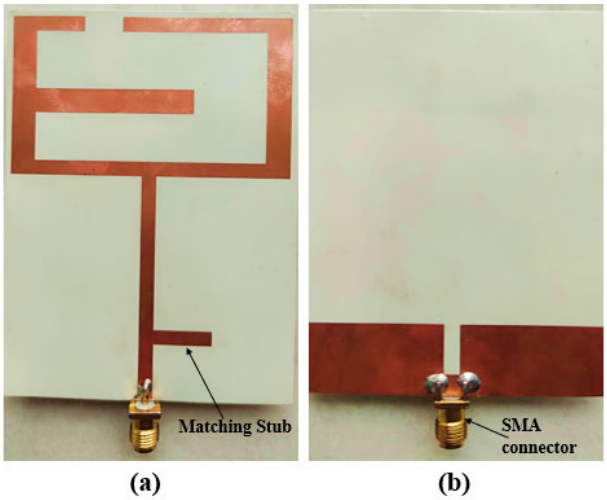


**FIGURE 14.** Fabricated antenna (a) Top (b) Back.

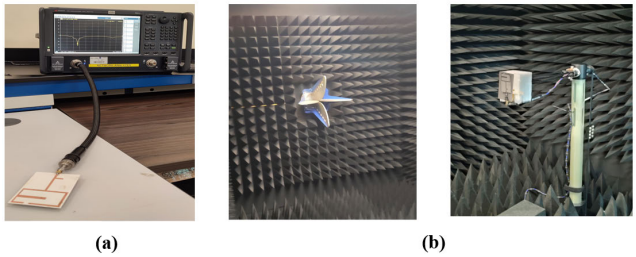


**FIGURE 15.** Measurement setup for the proposed antenna (a) $S_{11}$ measurement (b) Far-field measurements in anechoic chamber.

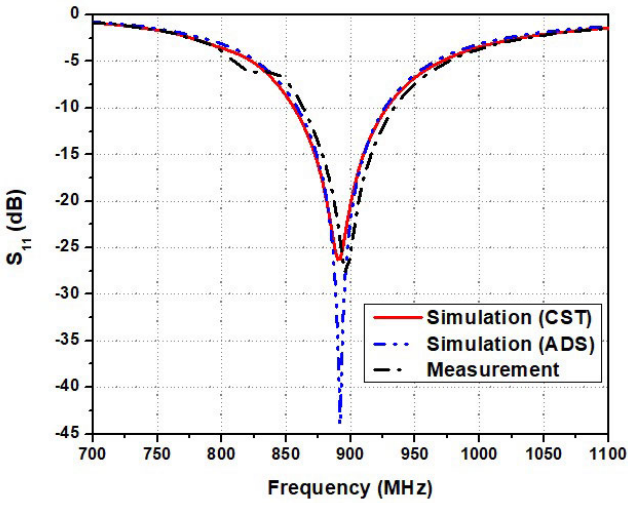


**FIGURE 16.** Comparison of $S_{11}$ of the proposed antenna for simulation, measurement, and equivalent circuit model.

anechoic chamber, shown in Fig. 15(b). During these tests, the proposed antenna functioned as the receiver, while a horn antenna was used as the transmitter, moving in both the azimuth and elevation planes. The analysis focuses on key metrics such as $S_{11}$, gain, radiation patterns, efficiency, and surface current distribution. To ensure the design's accuracy and reliability, a comprehensive comparison between the simulation and measurement results across these parameters was conducted.

### A. RETURN LOSS

The $S_{11}$ results of the proposed antenna, as shown in Fig. 16, compare the simulation model, equivalent circuit model, and measured prototype. Each model exhibits a return loss $<$ $-10$ dB with magnitude greater than $-25$ dB, sufficiently covering the bandwidth requirements of LoRa bands in various regions: Europe (867-869 MHz), North

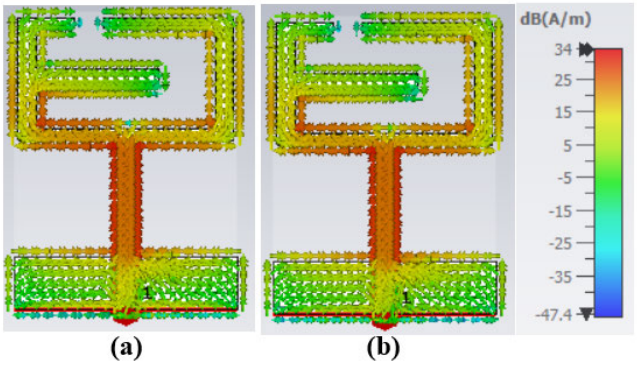


**FIGURE 17.** Current distribution characteristics of the proposed antenna (a) 868 MHz (b) 915 MHz.

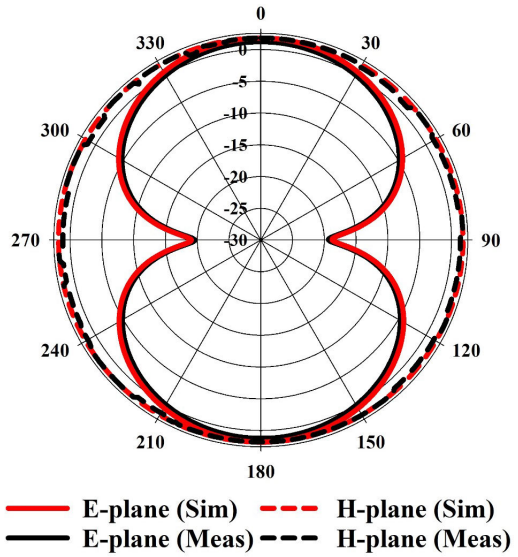


**FIGURE 18.** Radiation characteristics of the proposed antenna in *E-plane* and *H-plane*: (a) 868 MHz (b) 915 MHz.

America (902-928 MHz), Korea/Japan (920-925 MHz), and India (865-867 MHz). The figure demonstrates a satisfactory

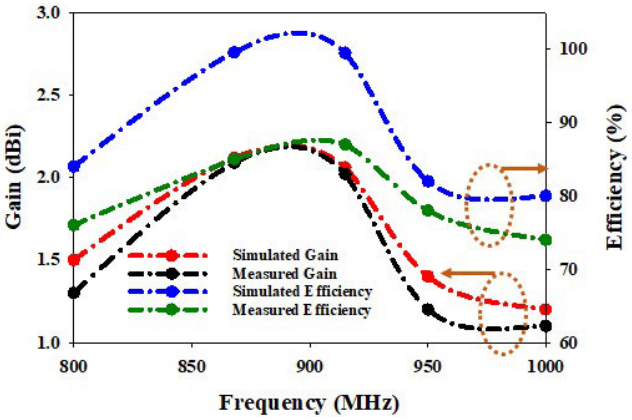


**FIGURE 19.** Gain and efficiency trends across different frequencies.

correlation among the $S_{11}$ results from the simulation, measurement, and equivalent circuit model.

### B. SURFACE CURRENT DISTRIBUTION ANALYSIS

The current distribution of the proposed antenna is depicted in Fig. 17. The maximum current density is concentrated around the feed line and the edges of the *U*-slot, as shown in Fig. 17(a) and (b). For each operational band (868 MHz and 915 MHz), the same elements are responsible for generating resonance. The surface current distributions validate the preliminary design of the antenna, which effectively generates resonances at both 868 MHz and 915 MHz through the conventional patch and the *U*-shaped slot. These findings are consistent with the theoretical principles discussed in an earlier study [30], which emphasize that the length of the current path on the patch influences the operational frequencies.

### C. ANALYSIS OF RADIATION CHARACTERISTICS

The radiation characteristics of the antenna are examined at both the 868 MHz and 915 MHz resonant frequencies. Fig. 18 illustrates the radiation patterns of the proposed antenna, comparing simulation and measurement results at these frequencies. In Fig. 18(a) and 18(b), corresponding to 868 MHz and 915 MHz respectively, bidirectional radiation patterns are evident in the *E*-plane, displaying an 'Eight' shape with a null lobe at $\theta = 90°$. Meanwhile, an omnidirectional pattern is observed in the *H*-plane. These characteristics hold for both simulated and measured data.

Fig. 19 presents plots of the antenna's gain and efficiency against frequency. Notably, the antenna exhibits nearly uniform gain (2.1 dBi) across all operational bands, with a peak radiation efficiency of 99.8% at 868 MHz. This suggests that the antenna is capable of transmitting and receiving signals with consistent strength across its operational frequency bands.

## VII. BENDING INVESTIGATION

When antennas are placed on the human body, they may experience bending. Therefore, it is crucial to investigate their

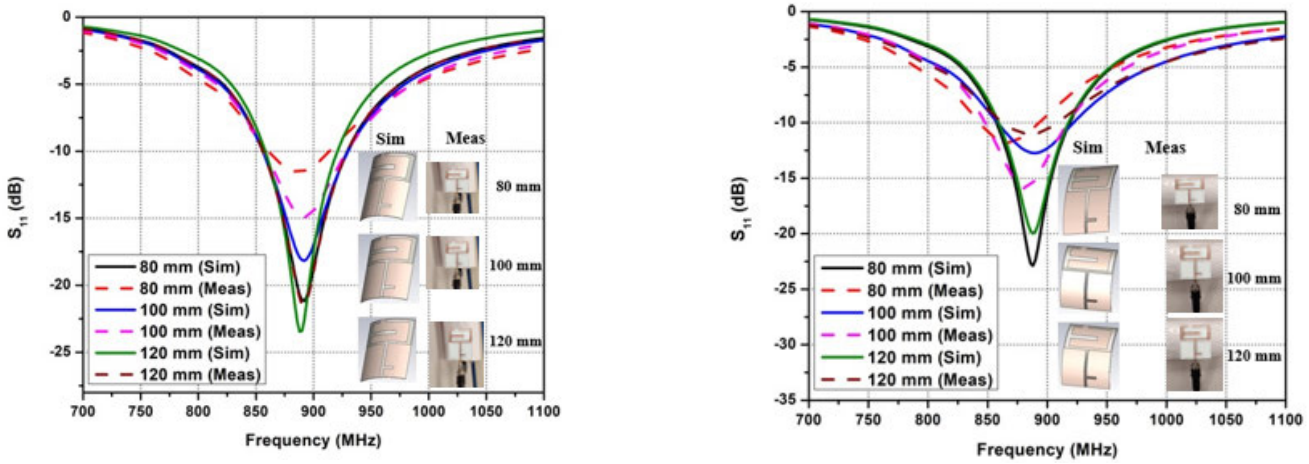


**FIGURE 20.** Bending investigation on the proposed antenna for various diameters (a) y-axis and (b) x-axis.

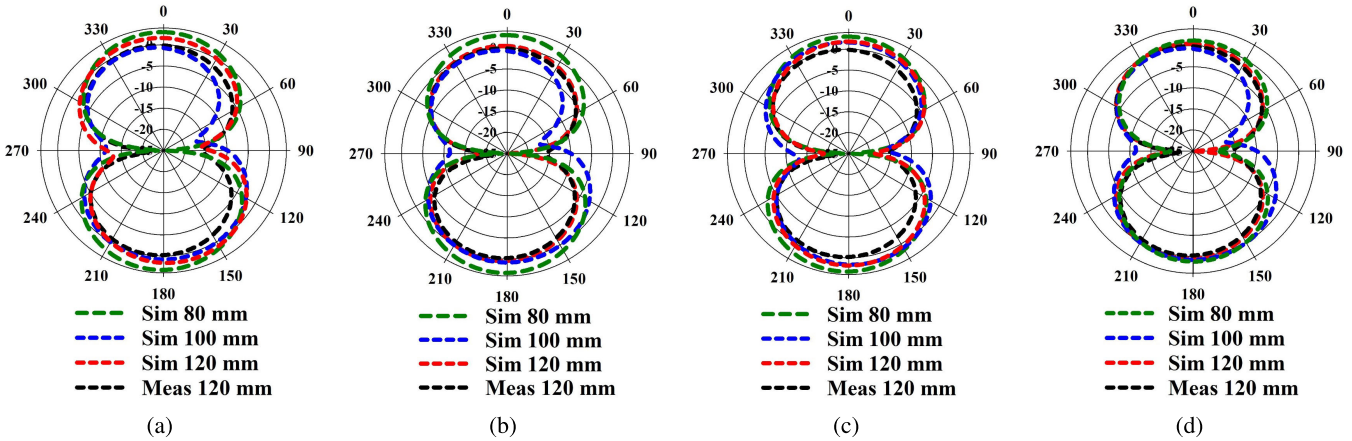


**FIGURE 21.** Comparison of radiation patterns under bending investigation on the proposed antenna for various diameters (a) 868 MHz (y-axis) (b) 868 MHz (x-axis) (c) 915 MHz (y-axis) and (d) 915 MHz (x-axis).

performance under bending conditions for WBAN applications. The bending investigation was conducted along both the y-axis and x-axis through simulations and measurements. The performance was analyzed for bending diameters of 80 mm, 100 mm, and 120 mm.

The simulated $S_{11}$ results as depicted in Fig. 20 were consistent for both the y-axis and x-axis. However, along the x-axis, a slight variation in $S_{11}$ was observed when the diameter decreased to 80 mm, although the antenna continued to operate at 868 MHz. For the measurements, Styrofoam was used to simulate bending conditions. It was found that the resonance frequencies shifted slightly for each Styrofoam diameter. Nonetheless, the impact was minimal, as the $-10$ dB bandwidth still covered the required 868 MHz and 915 MHz LoRa frequency bands. The simulation outcomes exhibited a notably higher level of accuracy compared to the measured results, possibly attributed to factors such as the utilization of Styrofoam, errors in fabrication, and losses in the cable connections.

Additionally, the radiation patterns were examined for various bending diameters ranging from 80 mm to 120 mm

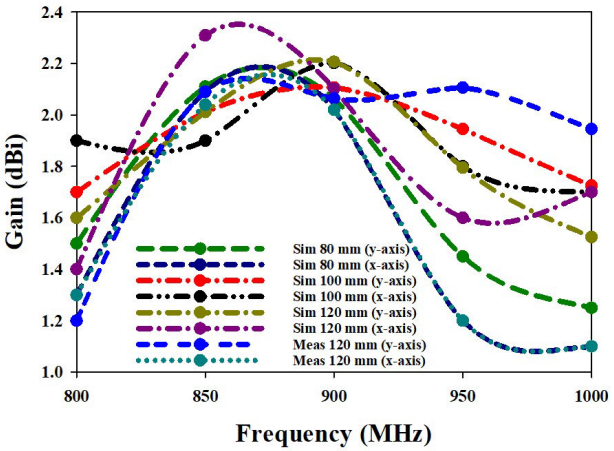


**FIGURE 22.** Plots of gains and efficiencies as functions of frequency under various bending conditions.

in simulations, while measurements were conducted using a 120 mm diameter, as illustrated in Fig. 21. The radiation patterns across different diameters showed consistent behavior with only minor deviations from the unbent scenario.

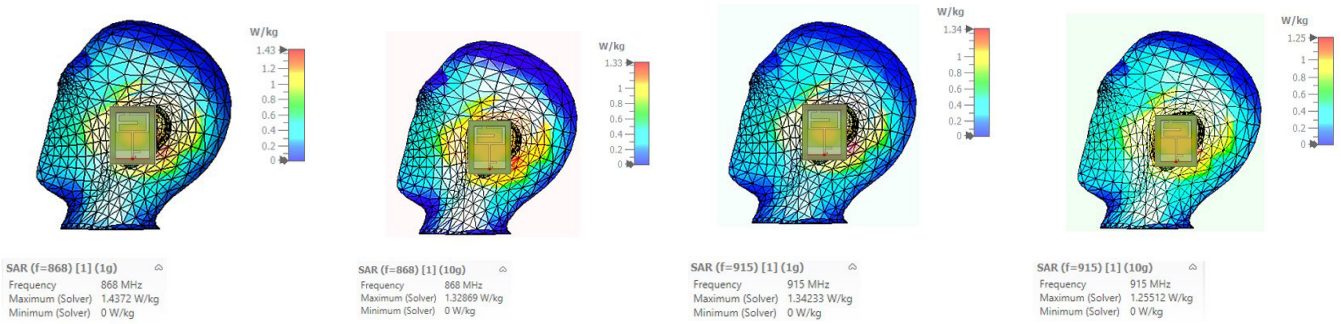


**FIGURE 23.** Simulated SAR values for the proposed antenna at (a) 868 MHz for 1 gram of tissue, (b) 868 MHz for 10 grams of tissue, (c) 915 MHz for 1 gram of tissue, and (d) 915 MHz for 10 grams of tissue.

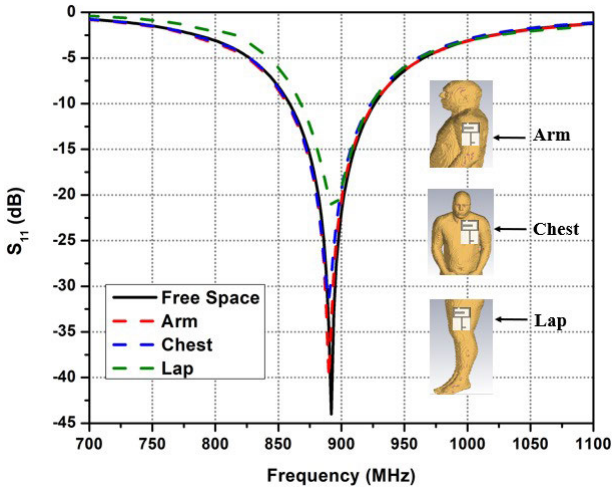


**FIGURE 24.** Simulated $S_{11}$ parameters of the proposed antenna in different scenarios: Free space, on the arm, on the chest, and on the lap.


**FIGURE 25.** Illustration of the proposed antenna when placed on the (a) chest (b) arm (c) lap.

These deviations are likely due to the minimal impact of bending on the antenna materials. The gain under bending conditions ranged from 1.1 dBi to 2.3 dBi along both the y-axis and x-axis for 868 MHz and 915 MHz, as depicted in Fig. 22. The results demonstrated a good correlation between the simulation and measurement data.

## VIII. SAR ANALYSIS

In designing antennas for WBAN applications, it is crucial to measure the Specific Absorption Rate (SAR) since the antenna may be positioned close to the human body [41]. SAR is a measurement that tells how much radiofrequency (RF) energy a body absorbs from a source [42], typically an antenna in this case. It's expressed as the rate of power absorbed per unit mass of tissue. According to FCC and ICNIRP standards, SAR must not exceed 1.6 W/kg for 1 g of tissue and 2 W/kg for 10 g of tissue [43], [44], [45]. These limits are calculated using the IEEE C95.1 standard in CST MWS® software.

To effectively determine SAR levels, the antenna's performance was evaluated on a human phantom. Fig. 23 illustrates the simulated SAR values for 1g and 10g of human tissue at the antenna's operating frequencies. As shown in Fig. 23(a) and 23(b), the SAR values at 868 MHz are 1.43 W/kg for 1g of tissue and 1.33 W/kg for 10g of tissue with an input power of 100 mW. Similarly, at 915 MHz, the SAR values are 1.34 W/kg for 1 g of tissue and 1.25 W/kg for 10 g of tissue, as depicted in Fig. 23(c) and 23(d). These results confirm that the antenna complies with FCC and ICNIRP standards for SAR limits.

## IX. EFFECT OF HUMAN BODY ON THE PROPOSED ANTENNA'S PERFORMANCE

Since the proposed antenna is intended for wearable applications and will be used in close proximity to the human body, it is crucial to examine the influence of the body on its performance. Fig. 24 presents the simulated $S_{11}$ parameters for the antenna when positioned on various parts of the body, including the arm, chest, and lap, as well as in free space. The findings demonstrate that the antenna consistently achieves the desired resonant frequencies of 868 MHz and 915 MHz across all tested scenarios.

Additionally, Fig. 25 illustrates the antenna's behavior when positioned on various parts of an actual human body, such as the lap, arm, and chest. The measured $S_{11}$ parameters for the antenna in these configurations, as depicted in Fig. 26, reveal a slight shift, particularly noticeable when the antenna is directly placed on the arm. This shift is attributed to the higher dielectric constant of human tissue, which affects the lower resonant frequencies.

The simulated radiation patterns of the proposed antenna when placed on different body parts like the chest, arm, and

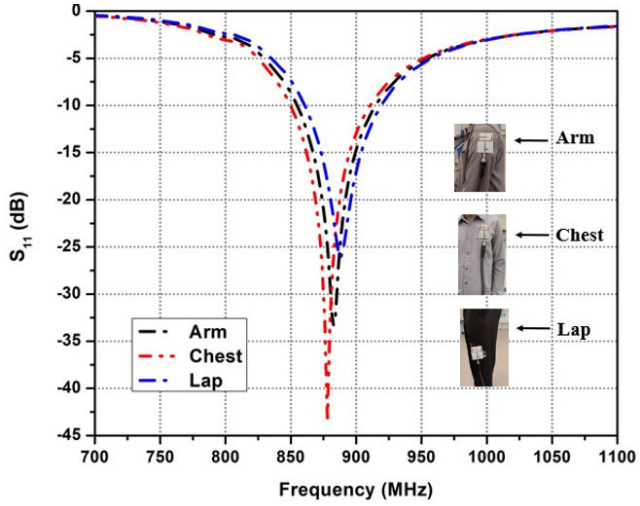


**FIGURE 26.** Performance of the proposed antenna showing its $S_{11}$ characteristics in free space and when placed on the chest, arm and lap.

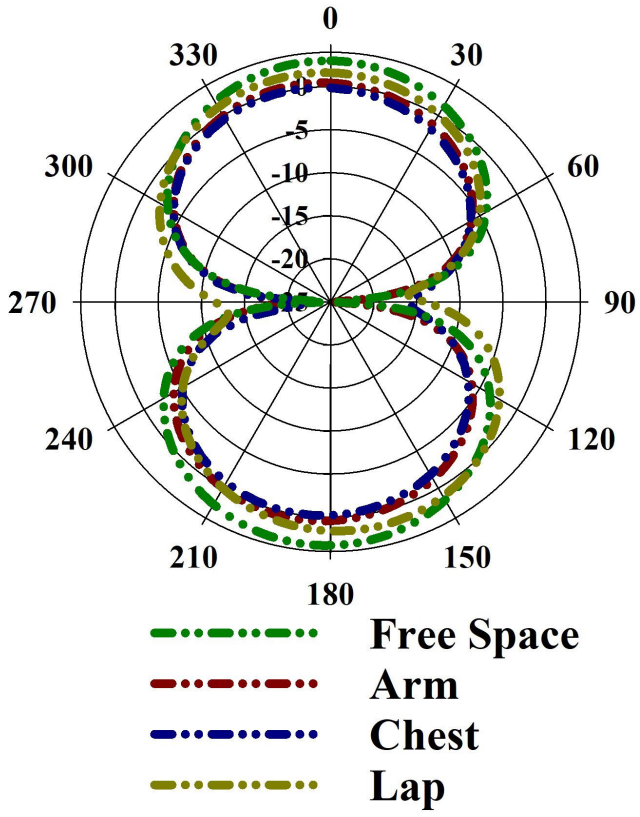


**FIGURE 27.** Simulated radiation patterns of the proposed antenna when placed on different parts of a human phantom at 868 MHz.

lap are displayed in Fig. 27 and Fig. 28. Both 868 MHz and 915 MHz exhibit minimal variation. This suggests the antenna's radiation characteristics are relatively insensitive to body placement.

Fig. 29 displays the simulated gain of the antenna on the arm, chest, and lap, ranging from 1.4 dBi to 2.3 dBi. This variation is influenced by the differing dielectric properties of these body areas. Despite these variations, the antenna

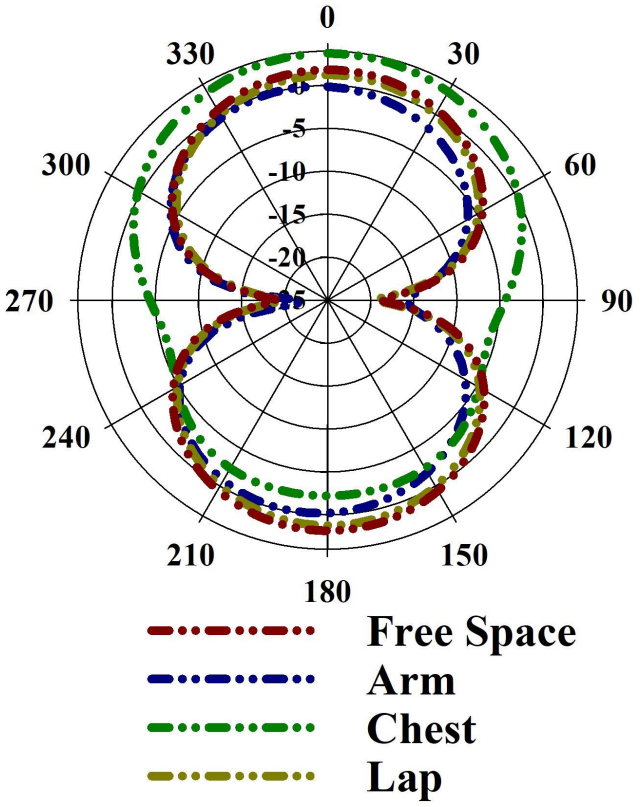


**FIGURE 28.** Simulated radiation patterns of the proposed antenna when placed on different of a human phantom at 915 MHz.

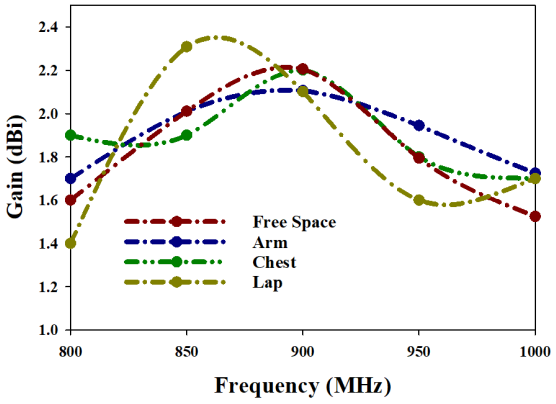


**FIGURE 29.** Gain of the antenna when placed on different parts of a human phantom at 868 MHz and 915 MHz.

maintains a consistent and acceptable level of performance across placements, ensuring reliable signal reception and transmission in wearable applications.

## X. EXPERIMENTAL VALIDATION

Vital indicators provide essential information about an individual's health status. Body temperature is a fundamental parameter, as deviations from the normal range can indicate various health issues, from infections to metabolic disorders. Similarly, heart rate is a critical indicator of cardiovascular health, with abnormal rates potentially signaling conditions such as arrhythmias, heart disease, or stress responses. The

proposed antenna's effectiveness for vital sign monitoring has been rigorously tested through a series of experimental validations. The focus was on monitoring key vital indicators such as body temperature and heart rate, which are critical for assessing the functioning of life-supporting processes and the severity of medical conditions.

### A. WBAN COMMUNICATION USING LORA

LoRa technology was chosen for WBAN communication due to its advantageous features. One key benefit is its non-cellular connectivity, allowing it to operate independently of cellular networks. This makes it particularly suitable for remote and rural areas where cellular coverage may be unreliable. Additionally, LoRa technology supports long-distance communication, with ranges extending up to several kilometers, ensuring reliable data transmission even in expansive environments. Another significant advantage is its low power consumption; LoRa devices are designed to use minimal power, making them ideal for battery-powered applications and extending the operational life of the devices. Furthermore, LoRa is particularly well-suited for IoT applications, providing robust and scalable connectivity solutions that enhance its utility in diverse scenarios [35], [46].

### B. EXPERIMENTAL SETUP

Conventional LoRa whip antennas, while effective for general applications, pose several challenges for WBAN use. Ergonomic issues arise because whip antennas are typically rigid and can be uncomfortable when worn on the body, potentially hindering the wearer's movement and comfort. Additionally, the size and shape of traditional whip antennas are not optimized for wearable applications, making them impractical for continuous use in a WBAN setting. These limitations necessitate the development of a more suitable antenna for wearable applications, prompting this study.

In this study, both the conventional LoRa whip antenna and the proposed antenna were utilized in the LoRa receiver (Rx) and transmitter (Tx) setups to evaluate their performance in monitoring vital signs. The experimental setup involved integrating the SEN11547 pulse sensor and the LM35 temperature sensor with the LoRa Tx. The SEN11547 pulse sensor was used to measure heart rate, while the LM35 temperature sensor measured body temperature. These sensors were connected to the LoRa Tx, which was responsible for transmitting the collected vital sign data. Once the sensors gathered the heart rate and body temperature data, this information was wirelessly transmitted from the LoRa Tx to the LoRa Rx. The LoRa Rx then displayed the received data along with the corresponding Received Signal Strength Indicator (RSSI) values. The RSSI provided an indication of the signal quality and strength, which is crucial for assessing the reliability of the communication link between the Tx and Rx. The experimental setup for the validation process are depicted in Fig. 30.

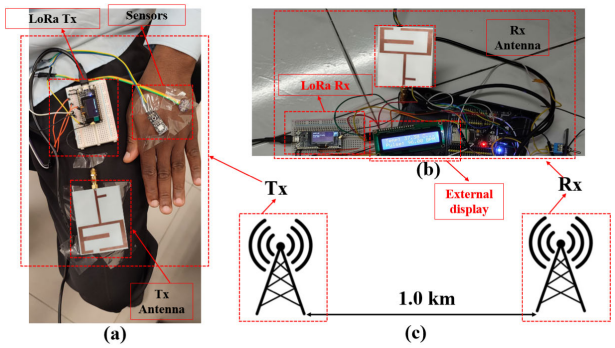


**FIGURE 30.** Validation setup.

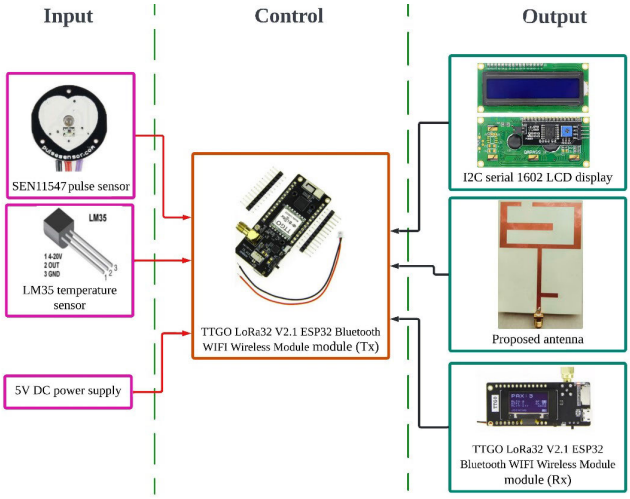


**FIGURE 31.** System block diagram.

### C. SYSTEM CONFIGURATION

The system block diagram of the proposed vital sign monitoring setup is illustrated in Fig. 31. This system integrates sensors, antennas, and SX1276 LoRa devices based on TTGO LoRa32 technology to facilitate efficient monitoring and data transmission. At the core of the system are the SEN11547 pulse sensor and the LM35 temperature sensor, which serve as input devices for measuring heart rate and body temperature, respectively. These sensors are connected to a LoRa device integrated with a microcontroller. The microcontroller, programmed using open-source Arduino IDE software, plays a crucial role in the system. The Arduino IDE, which is compatible with multiple operating systems, facilitates the coding process and enables easy uploading of sketches to boards. The LoRa technology ensures long-range, low-power communication, which is essential for reliable data transmission over significant distances. Upon receiving the signals, the LoRa Rx displays the measured heart rate and body temperature data along with the corresponding Received Signal Strength Indicator (RSSI) values, providing an immediate indication of the signal quality and reliability.

In the experimental setup, the position of the LoRa Rx was varied up to a distance of 1 km to evaluate the WBAN communication performance at 100 m intervals. It was observed that even at a distance of 1 km, the RSSI remained

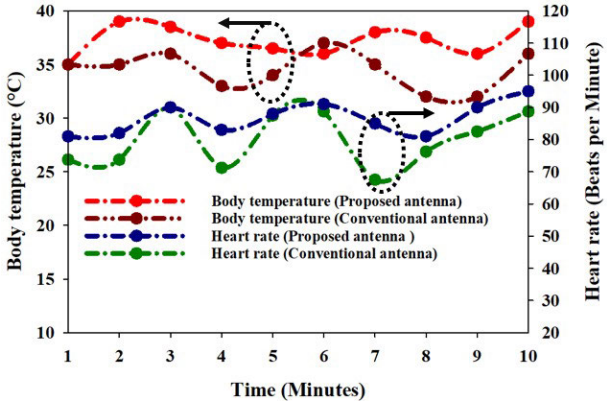


**FIGURE 32.** Comparison of measurements of heart rate and body temperature using the proposed antenna and commercially available conventional whip antenna.

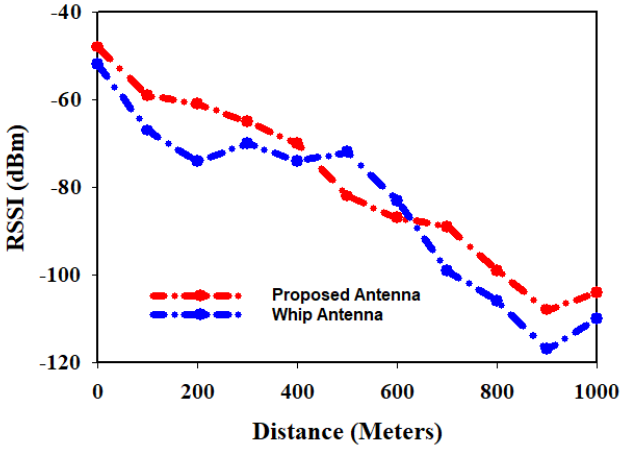


**FIGURE 33.** Comparison of RSSI values for the proposed antenna and the commercially available whip monopole antenna.

strong at −110 dBm, demonstrating the robustness and reliability of the proposed antenna and LoRa technology for WBAN applications. This setup highlights the practical advantages of using the proposed antenna in real-world scenarios, ensuring effective monitoring and communication over long distances without the limitations associated with conventional cellular-based systems. Previous studies have not explored using LoRa to establish WBAN communication, highlighting the novelty of this approach.

## XI. PERFORMANCE EVALUATION OF THE PROPOSED SYSTEM

To evaluate the performance of the proposed system, heartbeats and body temperatures were measured. Data were collected over a 10-minute period with samples taken every minute, resulting in 10 samples. These measurements were recorded under relaxed conditions, without any physical activity. For comparison and validation, the results were compared with those obtained using a conventional whip monopole antenna as a reference. Graphical representations of the vital signs measured are displayed in Fig. 32. It is evident from the figure that the measured heart rates ranged from 82 to 95 BPM. Despite these variations, all recorded values fell within the normal range for adults, which is between 60 and 100 BPM.

Additionally, body temperature data were collected and evaluated. An increase in body temperature is associated with a rise in heart rate, while a decrease in temperature corresponds to a slower heart rate. The recorded temperatures ranged from 35.20 to 38.80 °C, which is within the healthy range for adults (35 to 38 °C).

Overall, the analysis indicates a strong correlation between the measurements obtained using the proposed antenna and those obtained with the commercially available conventional monopole whip antenna. Minor variations in temperature readings can be attributed to measurement conditions.

To further validate the performance of the proposed antenna, the RSSI for each data packet was recorded at 100 m intervals using both the proposed antenna and a commercially available whip monopole antenna. The results, as presented in Fig. 33, show a consistent pattern. The overall comparison of RSSI indicates that the proposed antenna consistently demonstrates higher RSSI values across all distances when compared to the whip antenna. This suggests that the proposed antenna has superior signal reception capabilities. Both antennas exhibit a typical decrease in RSSI with increasing distance, which is expected due to path loss in wireless communications. However, the proposed antenna maintains a higher RSSI at each interval, indicating it is more efficient in mitigating signal loss over distance.

In examining performance at various distances, from 0 to 400 m, both antennas show a gradual decrease in RSSI, but the proposed antenna's RSSI remains about 5-10 dBm higher than that of the whip antenna. Between 400 and 800 m, the gap between the two antennas' performance widens slightly. The proposed antenna's superior performance is more pronounced, maintaining better signal strength. At distances from 800 to 1000 m, both antennas experience significant signal degradation, but the proposed antenna still performs better, indicating its robustness at longer distances.

In conclusion, the analysis of the RSSI data indicates that the proposed antenna outperforms the commercially available whip monopole antenna in all tested scenarios. The higher RSSI values across various distances suggest that the proposed antenna is more efficient in receiving signals and maintaining communication quality over extended ranges. Given these findings, the proposed antenna is highly effective for WBAN communications using LoRa technology, providing stronger and more reliable signal reception and making it a suitable choice for applications that require consistent and long-range wireless communication.

Table 8 compares the proposed antenna with antennas presented in recent literature. The proposed design offers a compelling alternative due to its compact size ($0.23\ \lambda_0 \times 0.17\ \lambda_0$), significantly smaller compared to other antennas utilizing semi-flexible, non-flexible, and flexible substrates. Notably, the proposed antenna achieves good performance across its operational bands (868 MHz and 915 MHz)

**TABLE 8.** Comparison of the performance of the proposed antenna with available literature.

| Ref. | Year | Bands | Method | Freq. (MHz) | Substrate | Dielectric ($\varepsilon_r$) | Patch | SAR* (W/Kg) | Gain (dBi) | Antenna Validated? | Size ($mm^2$) |
|---|---|---|---|---|---|---|---|---|---|---|---|
| [21] | 2021 | 2 | PIFA | 433<br>868 | Textile | 1.3 | Copper | 1.25<br>0.89 | 1.25 | No | 0.12 $\lambda_0$ × 0.25 $\lambda_0$ |
| [22] | 2021 | 1 | SIW | 867 | closed-cell rubber foam | 1.34 | Copper | 0.25 | −2.7 | No | 0.30 $\lambda_0$ × 0.27 $\lambda_0$ |
| [23] | 2023 | 2 | SIW | 867<br>915 | Rubber foam | 1.38 | Copper | 0.2 | −1.3<br>−0.6 | No | 0.37 $\lambda_0$ × 0.38 $\lambda_0$ |
| [47] | 2021 | 2 | MPA | 868<br>2400 | Neoprene | 1.95 | Silver | NA | 3.28<br>3.25 | No | 0.61 $\lambda_0$ × 0.61 $\lambda_0$ |
| [24] | 2022 | 2 | MPA/Slot | 867<br>915 | Wool felt | 1.4 | Copper | NA | NA | No | NA |
| **This work** | **2024** | **2** | **MPA/Slot** | **868<br>915** | **Rogers RO3003** | **3** | **Copper** | **1.43<br>1.34** | **2.06<br>2.12** | **Yes** | **0.23** $\lambda_0$ × **0.17** $\lambda_0$ |

with acceptable impedance bandwidth and promising gain values (2.06 dBi and 2.12 dBi). Furthermore, it features a bidirectional radiation pattern, making it suitable for LoRa WBAN communication applications. Crucially, this work goes beyond simulations to validate the antenna's performance. The proposed antenna was integrated into a functional LoRa system and employed for real-life vital sign measurements. This comprehensive validation process demonstrates the antenna's effectiveness in capturing and transmitting vital sign data through a LoRa communication link.

## XII. CONCLUSION

This work introduces a novel and compact wearable patch antenna specifically designed for monitoring vital signs in WBAN medical applications. The antenna operates within the globally prevalent LoRa bands of 868 MHz and 915 MHz, addressing a critical gap in the existing literature for compact wearable antennas suited for these specific sub-1 GHz bands. The fabrication utilizes a Rogers Duroid RO3003$^{TM}$ substrate, incorporating a U-slot on a traditional rectangular patch alongside a matching stub and partial ground plane for optimized impedance matching and enhanced performance efficiency. The resulting antenna boasts a compact size of 80 × 60$mm^2$ (0.23 $\lambda_0$ × 0.17$\lambda_0$), where $\lambda_0$ represents the free-space wavelength at 868 MHz. Additionally, the antenna exhibits a favorable radiation pattern, with a bidirectional pattern in the *E*-plane and an omnidirectional pattern in the *H*-plane, observed at both frequencies. The peak gain reaches 2.12 dBi at 868 MHz.

The design, simulation, and optimization processes leveraged the capabilities of CST MWS® software. Notably, this work integrates supervised regression machine learning models, particularly an ensemble regression model, to predict resonance frequencies based on various antenna parameters. This approach yielded remarkable accuracy, achieving an R-squared score of 87.68%. This success highlights the ensemble regression model's efficacy in predicting resonance frequencies, leading to reduced computational time requirements for full-wave simulations within CST MWS and a streamlined design process.

The antenna's performance was further evaluated by analyzing its characteristics under bending conditions. This assessment revealed that the antenna maintains excellent efficiency, with minimal degradation in bandwidth and gain even when subjected to bending. Additionally, a SAR analysis was conducted, ensuring all values fall well within the safety guidelines established by FCC and ICNIRP standards, demonstrating the antenna's suitability for wearable applications.

To validate performance in real-world settings, the fabricated prototype antenna underwent open-field testing for WBAN LoRa applications. Performance assessments were conducted using a LoRa transceiver system based on the LoRa SX1276 chip. The proposed antenna consistently surpassed a conventional antenna, demonstrating an average improvement of −5 dBm in Received Signal Strength Indication (RSSI) across various points within a 1 km range. This confirms the proposed antenna's superior signal reception capabilities, making it a promising solution for long-range WBAN applications, supported by robust performance metrics and comprehensive experimental validations.

## ACKNOWLEDGMENT

The authors would like to thank the Deanship of Scientific Research at Majmaah University for supporting this work under project number (R-2024-1210); and also would like to thank AlMaarefa University, Riyadh, Saudi Arabia, for supporting this research.

## REFERENCES

[1] M. N. Bhuiyan, M. M. Rahman, M. M. Billah, and D. Saha, "Internet of Things (IoT): A review of its enabling technologies in healthcare applications, standards protocols, security, and market opportunities," *IEEE Internet Things J.*, vol. 8, no. 13, pp. 10474–10498, Jul. 2021.

[2] W. Ayoub, A. E. Samhat, F. Nouvel, M. Mroue, and J.-C. Prévotet, "Internet of Mobile Things: Overview of LoRaWAN, DASH7, and NB-IoT in LPWANs standards and supported mobility," *IEEE Commun. Surveys Tuts.*, vol. 21, no. 2, pp. 1561–1581, 2nd Quart., 2019.

[3] T. N. Qureshi, Z. A. Khan, N. Javaid, A. Aldegheishem, M. B. Rasheed, and N. Alrajeh, "Elephant herding robustness evolution algorithm with multi-clan co-evolution against cyber attacks for scale-free Internet of Things in smart cities," *IEEE Access*, vol. 11, pp. 79056–79072, 2023.

[4] Y. B. Zikria, R. Ali, M. K. Afzal, and S. W. Kim, "Next-generation Internet of Things (IoT): Opportunities, challenges, and solutions," *Sensors*, vol. 21, no. 4, p. 1174, Feb. 2021.

[5] K. Shafique, B. A. Khawaja, F. Sabir, S. Qazi, and M. Mustaqim, "Internet of Things (IoT) for next-generation smart systems: A review of current challenges, future trends and prospects for emerging 5G-IoT scenarios," *IEEE Access*, vol. 8, pp. 23022–23040, 2020.
[6] M. Pérez, F. E. Sierra-Sánchez, F. Chaparro, D. M. Chaves, C.-I. Paez-Rueda, G. P. Galindo, and A. Fajardo, "Coverage and energy-efficiency experimental test performance for a comparative evaluation of unlicensed LPWAN: LoRaWAN and SigFox," *IEEE Access*, vol. 10, pp. 97183–97196, 2022.
[7] G. Pasolini, "On the LoRa chirp spread spectrum modulation: Signal properties and their impact on transmitter and receiver architectures," *IEEE Trans. Wireless Commun.*, vol. 21, no. 1, pp. 357–369, Jan. 2022.
[8] I. B. F. de Almeida, M. Chafii, A. Nimr, and G. Fettweis, "Alternative chirp spread spectrum techniques for LPWANs," *IEEE Trans. Green Commun. Netw.*, vol. 5, no. 4, pp. 1846–1855, Dec. 2021.
[9] M. S. Yahya, S. Soeung, S. K. A. Rahim, U. Musa, S. S. Ba Hashwan, Z. Yunusa, and S. A. Hamzah, "LoRa microstrip patch antenna: A comprehensive review," *Alexandria Eng. J.*, vol. 103, pp. 197–221, Sep. 2024.
[10] J. J. Kang, W. Yang, G. Dermody, M. Ghasemian, S. Adibi, and P. Haskell-Dowland, "No soldiers left behind: An IoT-based low-power military mobile health system design," *IEEE Access*, vol. 8, pp. 201498–201515, 2020.
[11] Y. Jain, B. Soni, A. Goyal, and C. Sharma, "Novel wearable device for health monitoring and tracking of soldiers based on LoRa module," in *Proc. IEEE 4th Conf. Inf. Commun. Technol. (CICT)*, Dec. 2020, pp. 1–5.
[12] H. Savci, H. Sajjad, S. Khan, and F. Kaburcuk, "Analysis of a compact multi-band textile antenna for WBAN and WLAN applications," *Balkan J. Electr. Comput. Eng.*, vol. 9, no. 3, pp. 255–260, Jul. 2021.
[13] T. Janssen, A. Koppert, R. Berkvens, and M. Weyn, "A survey on IoT positioning leveraging LPWAN, GNSS and LEO-PNT," *IEEE Internet Things J.*, 2023.
[14] J. J. Kang, "A military mobile network design: MHealth, IoT and low power wide area networks," in *Proc. 30th Int. Telecommun. Netw. Appl. Conf. (ITNAC)*, Nov. 2020, pp. 1–3.
[15] S. Lee, J. Lee, H.-S. Park, and J. K. Choi, "A novel fair and scalable relay control scheme for Internet of Things in LoRa-based low-power wide-area networks," *IEEE Internet Things J.*, vol. 8, no. 7, pp. 5985–6001, Apr. 2021.
[16] S. Bagwari, A. Gehlot, R. Singh, N. Priyadarshi, and B. Khan, "Low-cost sensor-based and LoRaWAN opportunities for landslide monitoring systems on IoT platform: A review," *IEEE Access*, vol. 10, pp. 7107–7127, 2022.
[17] A. K. Teshome, B. Kibret, and D. T. H. Lai, "A review of implant communication technology in WBAN: Progress and challenges," *IEEE Rev. Biomed. Eng.*, vol. 12, pp. 88–99, 2019.
[18] G.-P. Gao, B.-K. Zhang, J.-H. Dong, Z.-H. Dou, Z.-Q. Yu, and B. Hu, "A compact dual-mode pattern-reconfigurable wearable antenna for the 2.4-GHz WBAN application," *IEEE Trans. Antennas Propag.*, vol. 71, no. 2, pp. 1901–1906, Feb. 2023.
[19] H. M. Khater, F. Sallabi, M. A. Serhani, S. Turaev, and E. Barka, "Efficient hybrid fault-management clustering algorithm (HFMCA) in WBANs based on weighted bipartite graph," *IEEE Access*, vol. 11, pp. 57977–57990, 2023.
[20] N. F. Ibrahim, P. A. Dzabletey, H. Kim, and J.-Y. Chung, "An all-textile dual-band antenna for BLE and LoRa wireless communications," *Electronics*, vol. 10, no. 23, p. 2967, Nov. 2021.
[21] X. Wang, L. Xing, and H. Wang, "A wearable textile antenna for LoRa applications," in *Proc. IEEE 4th Int. Conf. Electron. Inf. Commun. Technol. (ICEICT)*, Aug. 2021, pp. 613–615.
[22] G. Muntoni, G. A. Casula, G. Montisci, T. Pisanu, H. Rogier, and A. Michel, "An eighth-mode SIW antenna for low-power wide-area network applications," *J. Electromagn. Waves Appl.*, vol. 35, no. 13, pp. 1815–1829, Sep. 2021.
[23] G. A. Casula, G. Montisci, and G. Muntoni, "A novel design for dual-band wearable textile eighth-mode SIW antennas," *IEEE Access*, vol. 11, pp. 11555–11569, 2023.
[24] R. Huang, W. Xia, L. Xing, and F. Zhu, "A dual-band footwear textile antenna for LoRa off-body communication," in *Proc. IEEE Conf. Antenna Meas. Appl. (CAMA)*, Dec. 2022, pp. 1–4.
[25] A. F. Alsager, "Design and analysis of microstrip patch antenna arrays," 2011.
[26] J. Zhang, J. Xu, Q. Chen, and H. Li, "Machine learning assisted antenna optimization with data augmentation," *IEEE Antennas Wireless Propag. Lett.*, 2023.
[27] G. James, D. Witten, T. Hastie, R. Tibshirani, and J. Taylor, "Linear regression," in *An Introduction to Statistical Learning: With Applications in Python*. Cham, Switzerland: Springer, 2023, pp. 69–134.
[28] A. Chakrabortty and T. Cai, "Efficient and adaptive linear regression in semi-supervised settings," 2017, *arXiv:1701.04889*.
[29] S. Banihashemi, G. Ding, and J. Wang, "Developing a hybrid model of prediction and classification algorithms for building energy consumption," *Energy Proc.*, vol. 110, pp. 371–376, Mar. 2017.
[30] M. S. Yahya, S. Soeung, S. K. A. Rahim, U. Musa, S. S. Ba Hashwan, and M. A. Haque, "Machine learning-optimized compact frequency reconfigurable antenna with RSSI enhancement for long-range ssPapplications," *IEEE Access*, vol. 12, pp. 10970–10987, 2024.
[31] F. Liu, X. Huang, Y. Chen, and J. A. K. Suykens, "Random features for kernel approximation: A survey on algorithms, theory, and beyond," *IEEE Trans. Pattern Anal. Mach. Intell.*, vol. 44, no. 10, pp. 7128–7148, Oct. 2022.
[32] A. N. Alkawaz, A. Abdellatif, J. Kanesan, A. S. M. Khairuddin, and H. M. Gheni, "Day-ahead electricity price forecasting based on hybrid regression model," *IEEE Access*, vol. 10, pp. 108021–108033, 2022.
[33] M. P. Haack, R. P. Jenkins, W. Mai, G. Mackertich-Sengerdy, S. D. Campbell, M. F. Pantoja, and D. H. Werner, "Physically realizable antenna equivalent circuit generation," *IEEE Access*, vol. 12, pp. 33652–33658, 2024.
[34] A. Roy, S. Bhunia, D. C. Sarkar, P. P. Sarkar, and S. K. Chowdhury, "Compact multi frequency strip loaded microstrip patch antenna with spur-lines," *Int. J. Microw. Wireless Technol.*, vol. 9, no. 5, pp. 1111–1121, Jun. 2017.
[35] M. S. Yahya, S. Soeung, F. Emmanuel Chinda, S. K. B. A. Rahim, U. Musa, N. B. M. Nor, and S. Cheab, "A compact reconfigurable multi-frequency patch antenna for LoRa IoT applications," *Prog. Electromagn. Res. M*, vol. 116, pp. 77–89, 2023.
[36] V. K. Pandey and B. R. Vishvakarma, "Theoretical analysis of linear array antenna of stacked patches," *84.40. Ua*, 2005.
[37] M. K. Meshram and B. R. Vishvakarma, "Gap-coupled microstrip array antenna for wide-band operation," *Int. J. Electron.*, vol. 88, no. 11, pp. 1161–1175, Nov. 2001.
[38] M. A. Haque, D. Saha, S. S. Al-Bawri, L. C. Paul, M. A. Rahman, F. Alshanketi, A. Alhazmi, A. H. Rambe, M. A. Zakariya, and S. S. Ba Hashwan, "Machine learning-based technique for resonance and directivity prediction of UMTS LTE band quasi Yagi antenna," *Heliyon*, vol. 9, no. 9, Sep. 2023, Art. no. e19548.
[39] Q. Wu, W. Chen, C. Yu, H. Wang, and W. Hong, "Machine learning-assisted optimization for antenna geometry design," *IEEE Trans. Antennas Propag.*, 2024.
[40] S. A. Babale, T. K. Geok, S. K. A. Rahim, C. P. Liew, U. Musa, M. F. Hamza, Y. A. Bakhuraisa, and L. Li Lim, "Machine learning-based optimized 3G/LTE/5G planar wideband antenna with tri-bands filtering notches," *IEEE Access*, vol. 12, pp. 80669–80686, 2024.
[41] H. Ş. Savcı and F. Kaburcuk, "FDTD-based SAR calculation of a wearable antenna for wireless body area network devices," *Int. J. Microw. Wireless Technol.*, vol. 15, no. 8, pp. 1354–1360, Oct. 2023.
[42] J. Trajkovikj and A. K. Skrivervik, "Diminishing SAR for wearable UHF antennas," *IEEE Antennas Wireless Propag. Lett.*, vol. 14, pp. 1530–1533, 2015.
[43] U. Musa, S. M. Shah, H. A. Majid, Z. Z. Abidin, M. S. Yahya, S. Babani, and Z. Yunusa, "Recent advancement of wearable reconfigurable antenna technologies: A review," *IEEE Access*, vol. 10, pp. 121831–121863, 2022.
[44] U. Musa, S. M. Shah, H. A. Majid, I. A. Mahadi, M. K. A. Rahim, M. S. Yahya, and Z. Z. Abidin, "Design and analysis of a compact dual-band wearable antenna for WBAN applications," *IEEE Access*, vol. 11, pp. 30996–31009, 2023.
[45] U. Musa, S. M. Shah, H. B. A. Majid, M. K. A. Rahim, M. S. Yahya, Z. Yunusa, A. Salisu, and Z. Z. Abidin, "Wearable dual-band frequency reconfigurable patch antenna for WBAN applications," *Prog. Electromagn. Res. M*, vol. 120, pp. 95–111, 2023.
[46] M. S. Yahya, S. Soeung, N. S. S. Singh, Z. Yunusa, F. E. Chinda, S. K. A. Rahim, U. Musa, N. B. M. Nor, C. Sovuthy, and G. E. M. Abro, "Triple-band reconfigurable monopole antenna for long-range IoT applications," *Sensors*, vol. 23, no. 12, p. 5359, Jun. 2023.
[47] N. F. Ibrahim, P. A. Dzabletey, H. Kim, and J.-Y. Chung, "An all-textile dual-band antenna for BLE and LoRa wireless communications," *Electronics*, vol. 10, no. 23, p. 2967, Nov. 2021.

**MOHAMED I. WALY** (Member, IEEE) received the degree in biomedical engineering and system baccalaureate, the M.Sc. degree in biomedical engineering and systems, and the Ph.D. degree from the Faculty of Biomedical Engineering and Systems, Cairo University, in 2004, 2009, and 2013, respectively. From 2004 to 2015 and from 2013 to 2015, he was a Consultant Engineer with CASBEC. Since October 2015, he has been an Assistant Professor with the Department of Medical Equipment Technology, College of Applied Medical Sciences, Majmaah University, Saudi Arabia. His current research interests include design microwave antennas for biomedical applications, machine learning applications in the medical field, prediction disease models, system dynamic models, and clinical engineering management systems.

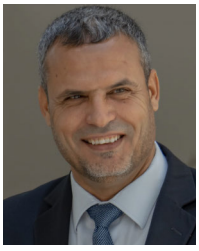

**JAMEL SMIDA** (Member, IEEE) received the degree in electrical engineering and the M.Sc. degree in electrical engineering from Tunis University, in 2000. Currently, he is affiliated with AlMaarefa University, Saudi Arabia, where he is the Quality Center Manager and a Lecturer with the Department of Computer Science. He is an Electrical Engineer and academic known for his contributions in the field of engineering and education. He is a Graduate Researcher with the Microwave Electronics Research Laboratory, Faculty of Mathematical, Physical and Natural Sciences of Tunis, University of Tunis El Manar, Tunisia. His research interests include deep learning, biomedical engineering, and educational quality assurance. He received the Aptitude Certificate for Technology Education, in 1995.

**MOHSEN BAKOURI** (Senior Member, IEEE) received the Ph.D. degree in systems and control engineering from the University of New South Wales (UNSW), Sydney, NSW, Australia, in 2014. He is currently a Professor with the Department of Biomedical Equipment Technology, Majmaah University, Saudi Arabia. He has authored or co-authored more than 50 papers and abstracts in international journals and conferences. This research has been multidisciplinary, involving techniques ranging from the design of sophisticated control applications in biomedical engineering to computational modeling and systems identification and bio-signal processing. His research interests include bio-signal processing, modeling, cardiovascular system control, and other mathematical modeling techniques.

**BAKHEET AWAD ALRESHEEDI** received the Ph.D. degree in nanomaterials engineering from the University of Dayton and The Ohio State University. He is currently an Assistant Professor with the Department of Biomedical Equipment Technology, Majmaah University, Saudi Arabia. He has co-authored more than 12 papers and abstracts in international journals and conferences. This research has been multidisciplinary, involving techniques ranging from the design of control applications in biomedical engineering to computational modeling and systems identification and bio-signal processing and electrical properties at different nanomaterials. His research interests include characterization of material in biomedical, such as system control and other mathematical modeling techniques.

**TARIQ MOHAMMED ALQAHTANI** received the Ph.D. degree in biomedical engineering from the University of Exeter, U.K. He is currently an Associate Professor with the Department of Biomedical Equipment Technology, Majmaah University, Saudi Arabia. He has authored two research papers and co-authored more than six papers and abstracts in international journals and conferences. His research interests include medical technology management, such as medical equipment replacement and medical device risk management.

**KHALID A. ALONZI** (Member, IEEE) received the Ph.D. degree in bioengineering from the University of New South Wales (UNSW), Sydney, NSW, Australia, in 2015. He is currently a Consultant Specialist with the Department of Biomedical Equipment Technology, HSMSD, Saudi Arabia. He has authored or co-authored more than 15 papers in international journals and conferences. This research has been multidisciplinary, involving techniques ranging from the design of sophisticated control applications in biomedical engineering to computational modeling and systems identification and bio-signal processing. His research interests include bio-signal processing, modeling, cardiovascular system control, and other mathematical modeling techniques.

**AMOR SMIDA** (Member, IEEE) received the degree in electronic baccalaureate and the M.Sc. degree in analysis and digital processing of electronic systems, in 2008 and 2010, respectively, and the Ph.D. degree from the Faculty of Mathematical, Physical and Natural Sciences of Tunis, University of Tunis El Manar, Tunisia, in 2014. From 2008 to 2014, he was a Graduate Student Researcher with the Unit of Research in High Frequency Electronic Circuits and Systems. Since August 2014, he has been an Assistant Professor with the Department of Medical Equipment Technology, College of Applied Medical Sciences, Majmaah University, Saudi Arabia. His current research interests include smart antennas and biosensors.